University of Kent

Kent Academic Repository

Currie, Andrew (2021) *Investigating the potential of Succinate dehydrogenase as an anti-fungal drug target in Candida glabrata.* Master of Research (MRes) thesis, University of Kent,.

Downloaded from
https://kar.kent.ac.uk/86837/ The University of Kent's Academic Repository KAR

The version of record is available from
https://doi.org/10.22024/UniKent/01.02.86837

This document version
UNSPECIFIED

DOI for this version

Licence for this version
UNSPECIFIED

Additional information

Versions of research works

Versions of Record
If this version is the version of record, it is the same as the published version available on the publisher's web site. Cite as the published version.

Author Accepted Manuscripts
If this document is identified as the Author Accepted Manuscript it is the version after peer review but before type setting, copy editing or publisher branding. Cite as Surname, Initial. (Year) 'Title of article'. To be published in *Title of Journal* , Volume and issue numbers [peer-reviewed accepted version]. Available at: DOI or URL (Accessed: date).

Enquiries
If you have questions about this document contact ResearchSupport@kent.ac.uk. Please include the URL of the record in KAR. If you believe that your, or a third party's rights have been compromised through this document please see our Take Down policy (available from https://www.kent.ac.uk/guides/kar-the-kent-academic-repository#policies).

Investigating the potential of Succinate dehydrogenase as an anti-fungal drug target in *Candida glabrata*

A thesis submitted to the University of Kent for the degree of

M.Sc. Cell Biology in the Faculty of Science, Technology and Medical Studies

2019/2020

Andrew Currie

School of Biosciences

Declaration

No part of this thesis has been submitted in support of an application for any degree or qualification of the University of Kent or any other University or institute of learning.

Andrew Currie

August 2020

Acknowledgements

I would like to thank my supervisor Dr Campbell Gourlay for the endless support and guidance throughout this project. Without his vast knowledge, this study would not have been possible. My gratitude also goes to the entirety of the Kent Fungal Group who have inspired me along the way.

Contents

TABLE OF CONTENTS

List of figures

Abbreviations

ACO1	Aconitase
AOX	Alternative oxidase
ATP	Adenosine triphosphate
BT	Blue tetrazolium
C. albicans	*Candida albicans*
C. glabrata	*Candida glabrata*
CDR1	*Candida* drug resistance
CIT3	Citrate synthase
CV	Crystal violet
DMSO	Dimethyl sulfoxide
EPA	Epithelial adhesin
ETC	Electron transport chain
FAD	Flavin adenine dinucleotide
FADH2	Flavin adenine dinucleotide hydrogen
FCCP	Mitochondrial oxidative phosphorylation uncoupler
FUM1	Fumarase
GPI	Glycosylphosphatidylinositol
H2DCF-DA	2',7'-dichlorodihydrofluorescein diacetate

IC	Invasive candidiasis
ICL1	Isocitrate lyase
IDH2	Isocitrate dehydrogenase
KCl	Potassium chloride
KGD1	α-ketoglutarate dehydrogenase
LiAC	Lithium acetate
LND	Lonidamine
LSC1	Ligase of Succinyl-CoA (alpha subunit)
LSC2	Ligase of Succinyl-CoA (beta subunit)
Mg_2SO_4	Magnesium sulfate
MITO-LND	Mitochondrially targeted Lonidamine
MLS1	Malate synthase
MTT	3-(4,5-dimethylthiazol-2-yl)-2,5-diphenyltetrazolium bromide
Na2CO3	Sodium Carbonate
NaH_2PO_4	Sodium dihydrogen phosphate
Na_2HPO_4	Sodium phosphate dibasic
NAD+	Nicotinamide adenine dinucleotide
NADH	Nicotinamide adenine dinucleotide hydrogen
NDE1/2	Mitochondrial external NADH dehydrogenase
NDI1	NADH Dehydrogenase Internal

NPA	3-nitropropionate
OD	Optical density
ONPG	Ortho-Nitrophenyl-β-galactoside
ORF	Open reading frame
PBS	Phosphate Buffer Saline
PDH1	Pleomorphic drug resistance
PEG	Polyethylene glycol
PI	Propidium iodide
PMS	Phenazine Methosulfate
RPM	Revolutions per minute
S. cerevisiae	*Saccharomyces cerevisiae*
SD	Synthetically defined
SDH	Succinate Dehydrogenase
TCA	Tricarboxylic acid cycle
TET	Triethyltin Bromide
TTFA	Thenoyltrifluoroacetone
URA	Uracil
WT	Wild type
YPD	Yeast peptone dextrose

Abstract

Candida glabrata is an opportunist human fungal pathogen which causes disease in immuno-compromised patients and is highly drug resistant to commonly prescribed anti-fungal drugs such as Fluconazole. This project tested whether Lonidamine (LND) has potential as a new antifungal agent. LND has shown to be safe in the mouse model so suggests it can be used in humans and has also recently been shown to inhibit Succinate dehydrogenase (complex II of the mitochondrial respiratory chain). LND caused a reduction in the *C. glabrata* biofilm and its ability to form colonies. Flocculation during growth assays suggested that LND causes disruptions of the cell wall. Respirometry analysis suggested LND does not utilise the ETC when SDH is inhibited and relies on the compensatory metabolic pathway known as the glyoxylate cycle. Through *S. cerevisiae* mutant studies, weak points within metabolic pathways were found to be ICL1 (within the glyoxylate cycle) and LSC2 (within the TCA cycle). Future research on combinational drug therapy of using LND alongside inhibitors of ICL1 or LSC2 would be crucial.

1. Introduction

1.1 *C. glabrata and S. cerevisiae* cellular structure

Many yeasts, such as *S. cerevisiae*, are harmless and used in a variety of food and bioprocessing processes. Others, such as *C. glabrata*, are pathogens that represent a real clinical threat. Yeasts are eukaryotes and such they share conserved biochemical processes and intracellular compartments with human cells. This represents a problem when it comes to designing drugs to target fungal pathogens. The conservation means that components such as signalling receptors, enzymes, transporters, motor proteins, protein or DNA synthesis regulators that might normally act as good targets for drug development in prokaryotes are more problematic as they may prove toxic. All yeasts contain a thick cell wall which acts as a defensive mechanism to external factors, and this structure is not found in mammalian cells. The cell wall is therefore one of the primary targets for anti-fungal drugs that are currently used in the clinic. The cell wall is composed of an outer facing oligosaccharide layer which connects to mannoproteins and has an underlying matrix of glucan and chitin. The echinocandin class of antifungals targets the enzyme 1,3-β glucan synthase and so impairs cell wall synthesis. The cell wall is anchored to the plasma membrane via glucan connections and contains integral proteins responsible for cell wall synthesis.

Ergosterol is a sterol which is found within fungi but not mammalian cells. It regulates both the membrane fluidity and structure. This highlights another target which is good for anti-fungal drugs and the azole class of drugs utilise this. The available antifungal classes interfering with ergosterol synthesis affect the products of the *ERG11* gene (14α-demethylase; azoles), the *ERG1* gene (squalene epoxidase; allylamines), and the *ERG2* gene (sterol C-8 isomerase; morpholines). The potential of the 22 remaining genes required for ergosterol biosynthesis as antifungal targets remains to be explored (Rodrigues, 2018). Fluconazole which is the most commonly prescribed antifungal drug has mechanisms of actions that inhibit the cytochrome P450 enzyme lanosterol demethylase (14α-demethylase), encoded by *ERG11*, in the ergosterol biosynthesis pathway. This prevents ergosterol biosynthesis and consequently produces toxins as methylated sterols accumulate within the fungal cellular membrane.

In the US, *C. glabrata* have higher rates of fluconazole resistance (11–13%) than *C. albicans* (0.5–2%), *C. tropicalis* (4–9%) and *C. parapsilosis* (2–6%) (Cleveland *et al.*, 2012). In the UK, the inherent drug resistance of *C. glabrata* has risen, while *C. albicans* resistance has not risen above 1% for fluconazole in England in 2018 (Public Health England, 2017). *C. glabrata* susceptibility test results to *C. glabrata* isolates over the years of 2015-2017 show that voriconazole and fluconazole resistance has fluctuated, between 13% - 17% for voriconazole, and 12% - 20% for fluconazole (Public Health England, 2017). This further provides evidence for need of new development of new drug target.

1.2 *Candida* species as human fungal pathogens

Candida are among the most common human pathogenic fungi; the majority of the human population carries members of the genus *Candida* on their mucous membranes. The overwhelming majority (>90%) of Candida infections are caused by only four species: *C. albicans* (>50% of all cases), *C. glabrata*, *C. parapsilosis*, and *C. tropicalis*. *C. albicans, C. parapsilosis and C. tropicalis* belong to the CTG clade, a phylogenetic group that translates the CTG codon into serine instead of leucine (Butler *et al*., 2009).

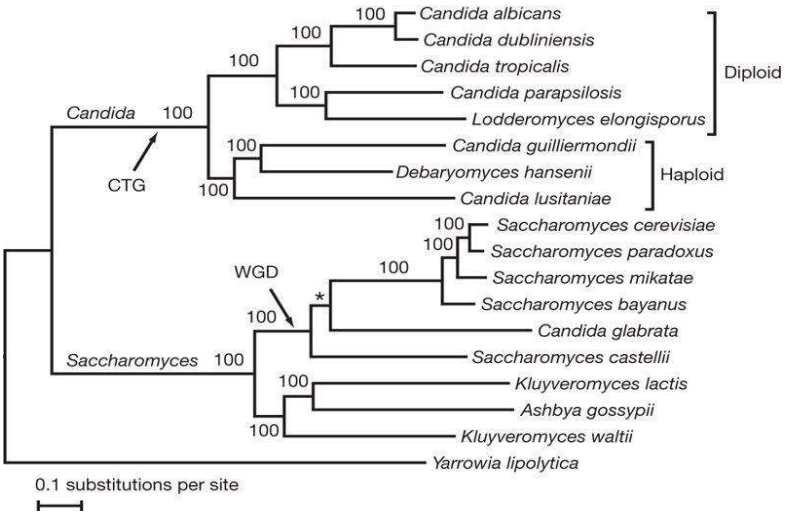

Figure 1. Phylogeny of sequenced Candida and Saccharomyces clade species. The asterisk marks a branch that was constrained on the basis of syntenic conservation (Butler *et al*., 2009)

Mucosal infections, known as Candidiasis but more commonly as thrush, are easily treated in most cases but can be associated with significant morbidity. *Candida* bloodstream infections, also known as Candidemia, are difficult to treat and associated with a high mortality which can remain as high as 40% (Kullberg

and Arendrup, 2015). Although *C. albicans* represents the most prevalent human fungal pathogen, the variations in mortality and geographical spread are reported. For example it has been noted mortality can be higher in patients with *Candida* species that aren't *C. albicans* compared to *C. albicans* itself (Montagna *et al.*, 2014) and *C. glabrata* is commonly isolated in the German-speaking countries, France, UK and North Europe; *C.parapsilosis* is more highly represented in Turkey, Greece and Spain (Montagna *et al.*, 2014).

Invasive candidiasis (IC) is a leading cause of mycosis-associated mortality in the United States. Candidiasis was the cause for approximately 0.4 deaths per 100,000 population, since 1997 (Pfaller and Diekema, 2007). *C.glabrata* has emerged as the second most common cause of IC in the United States (Pfaller and Diekema, 2007). This data highlights the crucial importance of keeping a wider scope of research for fungal pathogens.

1.3 Biofilms as a virulence factor associated with *Candida glabrata*

C. glabrata is able *to* form a biofilm and this has been linked to its pathogenicity (Fidel, Vazquez and Sobel, 1999) and drug resistance as it has been shown that cells in the biofilm environment are up to 1000-fold more azole resistant than their planktonic counterparts, making azoles an ineffective biofilm treatment option (Ramage *et al.*, 2012). These extracellular matrix-embedded structures appear on both biotic and abiotic surfaces. *C. glabrata* utilise biofilms as a means of antifungal resistance and they do this by compacting a dense

structure of yeast cells nested within the extracellular matrix. *C. glabrata* has a unique biofilm which is high in both protein and carbohydrates whilst the *C. parapsilosis* biofilm matrices have large amounts of carbohydrate with less protein. Conversely, matrices extracted from *C. tropicalis* biofilms had low amounts of carbohydrate and protein (Silva *et al.*, 2009). The high abundance of carbohydrates and proteins can act as a rich nutrient source within the biofilm that can allow for more than one species to co-exist within the biofilm in a synergistic manner.

The ability to adhere to host tissue and initiate a biofilm relies on adhesins, such as the cell wall associated glycosylphosphatidylinositol (GPI) proteins (de Groot *et al.*, 2008) . GPI proteins have an N-terminal ligand-binding sight along with a simple serine and threonine-rich region. These have tandem repeats which end with a C-terminus GPI-anchor attachment (de Groot *et al.*, 2008). The epithelial adhesin EPA1 gene is suggested to be the most important role in the adhesion of *C. glabrata* to epithelial cells (Sundstrom, 2002). Following adherence to the host, cell division and proliferation leads to the forming of a basal layer of anchoring microcolonies (Silva *et al.*, 2012).

1.4 Drug resistance in *C. glabrata*

C. glabrata has a natural multidrug (MDR: azole + echinocandin) adaptive resistance (Healey and Perlin, 2018). Currently azole resistance for *C. glabrata* isolates is 8% (Castanheira *et al.*, 2017) but the worrying statistic is that whilst echinocandin therapy has shown to be highly efficacious against *C. glabrata,* a

study which looked at 313 *C. glabrata* isolates from Duke Hospital showed that resistance to echinocandins increased from 4.9% to 12.3% in just a space of 9 years (Alexander *et al.*, 2013). Despite having a range of mechanisms for drug resistance, *C. glabrata* has shown to utilise the upregulation of multidrug transporters such as the CDR1 and PDH1, with preference for the latter having been shown (Vermitsky *et al.*, 2006). The resistance to echinocandins does not appear to be by the same mechanisms as overexpression of CDR1 showed no increase in resistance to micafungin or caspofungin (Niimi *et al.*, 2006).

In several fungal species, respiratory stress has been linked with increased resistance to azole drugs (Shingu-Vazquez and Traven, 2011). When mitochondrial function is impaired in *S. cerevisiae,* the transcription factor PDR3 functions to increase the expression of efflux pump encoding genes, such as the ABC drug transporter PDR5. In *C. glabrata* a similar phenomena has been observed via CgPDR1 upregulating CDR1 and CDR2 (Brun et al., 2004).

Increased drug resistance in *C. glabrata* correlates with increased virulence and fitness of the strains expressing mutated CgPDR1 via up regulation of the efflux pump activity (Ferrari et al., 2009). Clinical isolates of *C. glabrata* have also shown higher levels of drug resistance that correlates with mitochondrial dysfunction, which was verified in a mouse model of disease (Ferrari et al., 2011).

An article in 2004 (Vermitsky and Edlind, 2004) showed that *C. glabrata* induced upregulation of multidrug transporter genes CDR1 and PDH1 produced from rare mutations that are selected by drug pressure. As *C. glabrata* has shown resistance to commonly used clinical drugs such as azoles, the need to investigate other potential structures of the fungi have never been more important.

1.5 The mitochondria and associated metabolic pathways of *C. glabrata*

1.5.1 The mitochondria of *C. glabrata* as a new antifungal target

C. glabrata is a haploid budding yeast and has a mitochondrial genome which is relatively small and consists of only 8 ORFs (open reading frames) which code for the three subunits of Cytochrome C oxidase, the apocytochrome b, the three subunits of ATP synthase and the ribosomal protein VAR1. As well as 2 rNAs, 23 tRNAs and 1 non-coding RNA (Koszul *et al.*, 2003). A notable difference structurally in terms of the electron transport chain (ETC) to that of other *Candida* species is that it does not contain a multi-subunit Complex I or an AOX enzyme (Sun *et al.*, 2005). Respiration deficiency leads to attenuated virulence in the fungal pathogen (Brun *et al.*, 2005). This may make the respiratory chain a potentially easier target for mitochondrial inhibition than other fungal pathogens that possess alternative pathways. However, as its Crabtree positive,

inhibition of electron transport alone may not be sufficient. *C. glabrata* depend on oxidative phosphorylation for virulence.

Disruption of the respiratory pathway at selected points can increase intracellular levels of reactive oxygen species in yeast (Barros, Netto and Kowaltowski, 2003). It has been shown that yeast strains which lack mitochondrial function are sensitized to oxidative stress due to reactive oxygen species (ROS). Literature suggests that oxidant sensitivity is due to a defect in an energy requiring process which is needed for ROS detoxification or repair due to oxidative damage (Grant, MacIver and Dawes, 1997).

Recently, (Sun *et al.*, 2019) an article was published which highlighted seven genes of the CTG clade which show promising therapeutic targets after it was shown that these play crucial roles in the ETC pathway. The ETC function in the mitochondria has a role on pathogenesis, growth, anti-fungal susceptibility and yeast-to-hyphae in the cases of *C. albicans.* With the mounting pressure from resistant strains, the mitochondria have become the new limelight target for antifungal drugs.

Pharmacological approaches suggest that Antimycin A and Cyanide lead to inhibited growth and oxidative stress in *C. albicans* (Ruy, Vercesi and Kowaltowski, 2006). TTFA has shown to be a potent complex II inhibitor for the respiratory chain causing inhibition of mitochondrial respiration. Inhibition occurs by binding of TTFA to two ubiquinone binding sites, Qp and Qd. TTFA has been shown to cause a delay in overall cell cycle progression which consequently

leads to oxidative stress. Collectively, these points suggest that targeting the mitochondria could provide a promising therapeutic approach.

1.5.2 TCA and glyoxylate cycles

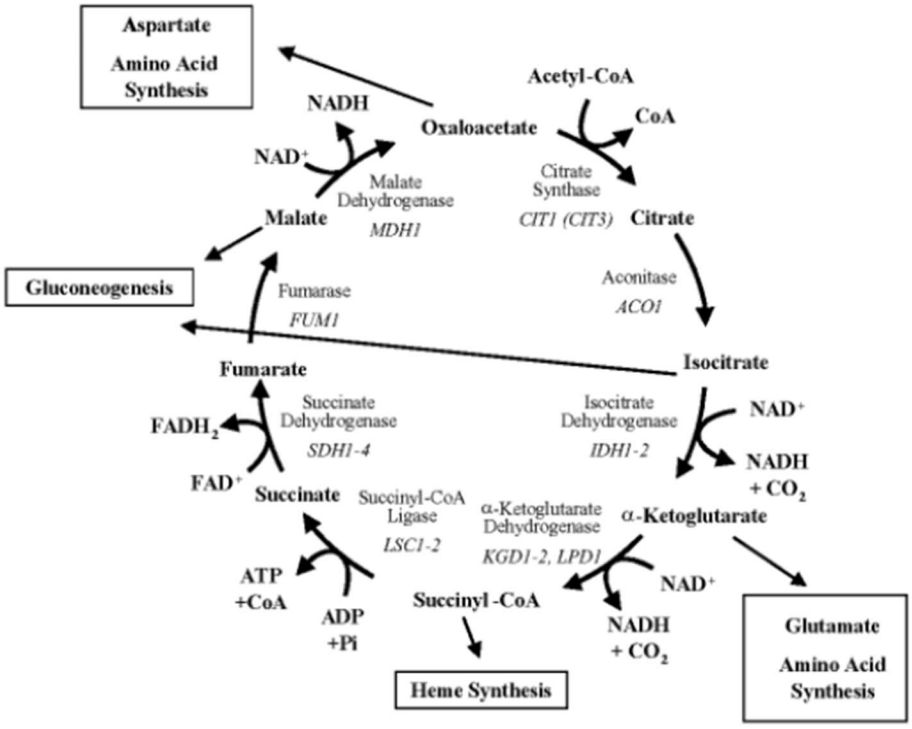

Figure 2. A schematic of the tricarboxylic acid cycle

Both *S. cerevisiae* and *C. glabrata* are able to live within aerobic and anaerobic conditions. With lacking oxygen, they can generate energy via glycolysis whereby glucose is broken down and converted to ethanol (less energetically favourable). With oxygen present, they can perform aerobic respiration whereby they glucose is broken down into CO^2 and ATP is generated by both the TCA (tricarboxylic acid) cycle and the ETC (electron transport chain). The TCA cycle utilises the molecule acetyl-CoA which is produced by the oxidation of pyruvate

(product of glucose metabolism). Through a series of redox reactions, the energy is generated through NADH, $FADH_2$ and ATP molecules along the cycle. It is the $FADH_2$ and NADH which are donated to the ETC for the more energetically favourable oxidative phosphorylation. Surprisingly, being Crabtree positive means that they opt to perform fermentation to generate their ATP rather than the energetically favourable TCA and ETC mechanisms, even when in very rich glucose medium.

Unlike mammalian cells, *C. glabrata* have a compensatory glyoxylate cycle which can provide intermediates back into the TCA cycle when it is dysfunctional. It also can be an adaptive mechanism for *C. glabrata* as it is an opportunist pathogen and can invade hosts which may not provide nutrient rich sources. The glyoxylate cycle allows for a certain degree of metabolic flexibility as it can utilise alternative carbon sources. Transcriptional analyses of macrophage engulfed *C. glabrata* have shown that key metabolic enzymes in the glyoxylate cycle were ICL1 and MLS1. (Chew, Chee and Than, 2019). This suggested that the microenvironment within the macrophage environment is deficient of glucose and initiated a metabolic switch within *C. glabrata.* It has been suggested already that engulfed *C. glabrata* cells utilise acetyl-CoA from the breakdown of fatty acids via the glyoxylate cycle as the main carbon source for the production of cellular building blocks (Rai *et al.*, 2012).

1.6 Fungal respiration as a potential anti-fungal target

1.6.1 Complex I inhibition

Several Complex I (NADH:ubiquinone oxidoreductase) subunits have been shown to be fungal specific (Sharma, Lu and Bai, 2009). Eukaryotic complex I has a core of 14 alpha-proteobacterial subunit proteins and a variable number of supernumerary subunit proteins. Of the latter group of proteins, one (NUZM) is fungal-specific, and a second (NUXM) is found in fungi, algae and plants but is not a mammalian complex I subunit protein. These subunit proteins have been designated as Nuo1p and Nuo2p (NADH-ubiquinone oxidoreductases) (She *et al.*, 2015). This highlights potential future drug targets which have yet to be fully investigated. Deletion of regulatory proteins of Complex I lead to both respiratory and virulence deficiencies in *C. albicans* (She *et al.*, 2015). Rotenone, which inhibits complex I, has been shown to cause cell death that is linked to the accumulation of ROS (Li *et al.*, 2011). Some yeasts, such as *S. cerevisiae* and *C. glabrata* do not possess a multi-subunit complex I and rely NADH dehydrogenase enzymes located on either the matrix or intermembrane space side of the inner mitochondrial membrane. The mitochondrial external NADH dehydrogenase are (NDE1 and NDE2) and a NADH Dehydrogenase Internal (NDI1).

Flavone, which is a specific inhibitor of the *S. cerevisiae* NDI1 has shown to inhibit almost completely NADH oxidase and NADH-UQ1 reductase activities of NDI1 (Kitajima-Ihara and Yagi, 1998).

1.6.2.1 Complex II (succinate dehydrogenase)

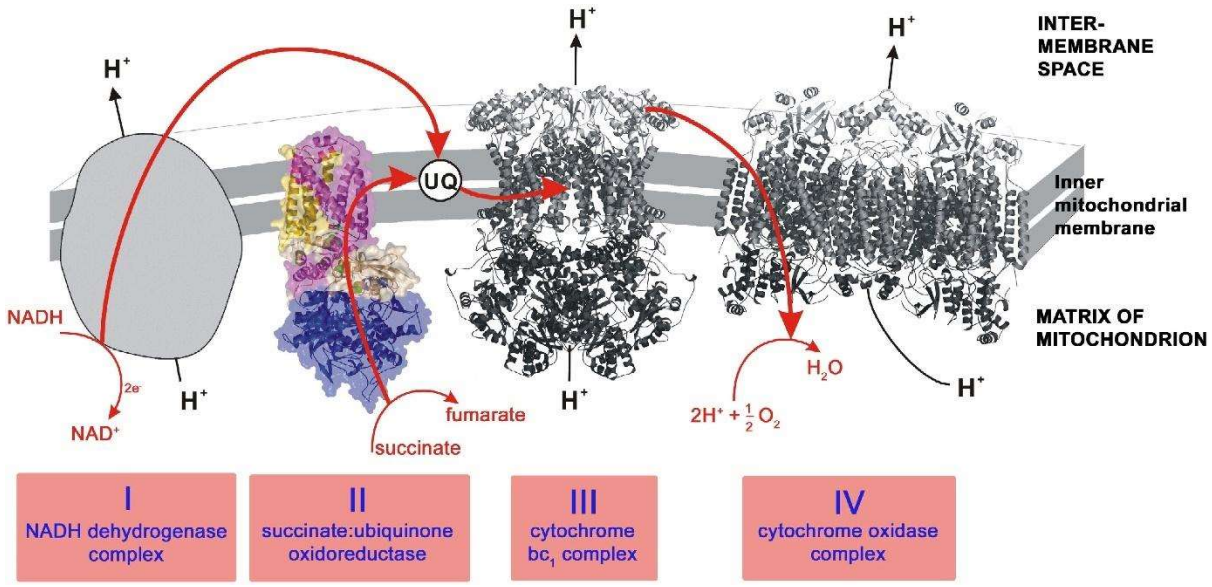

Figure 3. The role of Complex II in the Mitochondrial respiratory chain (Sun *et al*., 2005)

The mechanisms of complex II (succinate:ubiquinone oxidoreductase) begin with the catalysed oxidation of succinate to fumarate in the TCA which in turns donates electrons to ubiquinone in the inner mitochondrial membrane. The Succinate dehydrogenase (SDH) is crucial to aerobic respiration. SDH catalyses the oxidation of succinate into fumarate via the Krebs cycle. To note a differing factor is that it does not use soluble NAD+ intermediates. Succinate:ubiquinone oxidoreductases consist of a peripheral domain, exposed to the to the matrix in

the mitochondria and a membrane-integral domain that spans the membrane (Figure 3). The peripheral has a dicarboxylate binding site which consists of a flavoprotein and a covalently bound FAD. It is this FAD which is the substrate which removes two hydrogen electrons from the oxidation of succinate to fumarate. Three Iron-Sulfur clusters are present in the peripheral domain which are [2Fe-2S] cluster, a [4Fe-4S] cluster and a [3Fe-4S] cluster. The membrane-integral domain acts to anchor the flavoprotein and Iron-Sulfur subunits to the membrane and is required for quinone reduction and oxidation (Hägerhäll, 1997). It is suggested that electron transfer via the FAD substrate as $FADH_2$ then passes donated electrons through the iron sulphur clusters towards ubiquinone (Kregiel, 2012).

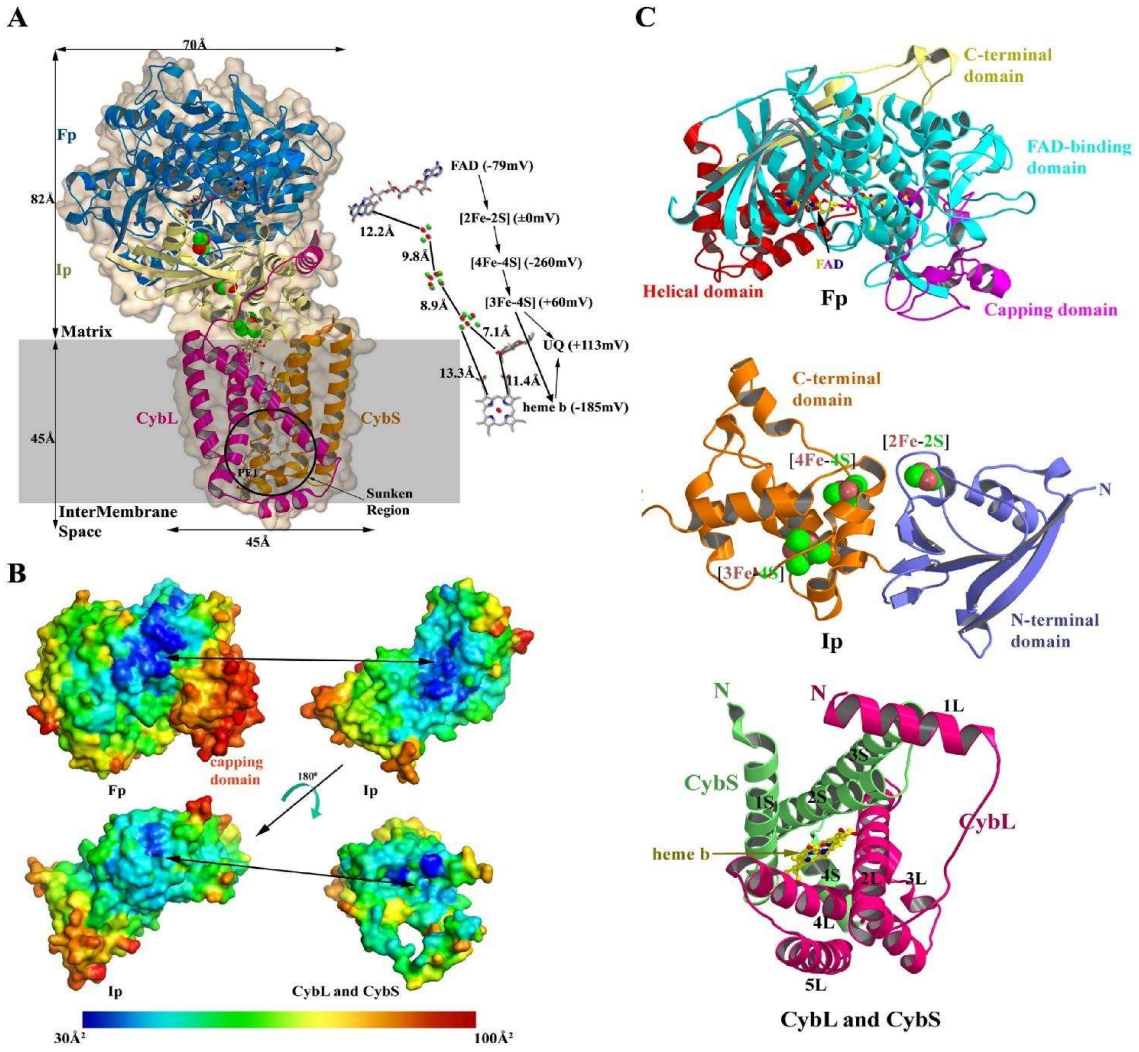

Figure 4. The Mitochondrial Respiratory Complex II Structure (Sun *et al*., 2005)

The Succinate oxidation is coupled with Ubiquinone to Ubiquinol as part of the electron transport chain (within the inner membrane). The Ubiquinone acts as an electron carrier to complex III. This entire process links respiration to the TCA cycle, which provides intermediates for biosynthesis of macromolecules in addition to its role in supporting respiration. What makes complex II a particularly interesting target for this project is how it acts as a member of both the TCA and the ETC, whereas other complexes are simple electron carriers by

a simpler means of NADH to form an electrochemical gradient across the inner mitochondrial membrane necessary for ATP production.

The SDH enzyme is sensitive to thiol groups which originally have been shown to not play much importance in the binding or catalysis activity (Kregiel, 2012). As previously stated, Inhibitors of Complex II include TTFA which inhibits its quinone reduction activity by occupying its ubiquinone binding sites. It is shown (Figure 5C and 5D) that TTFA molecules are found in the proximity of [3Fe-4S] and at the distal side of the transmembrane anchor (Sun *et al.*, 2005).

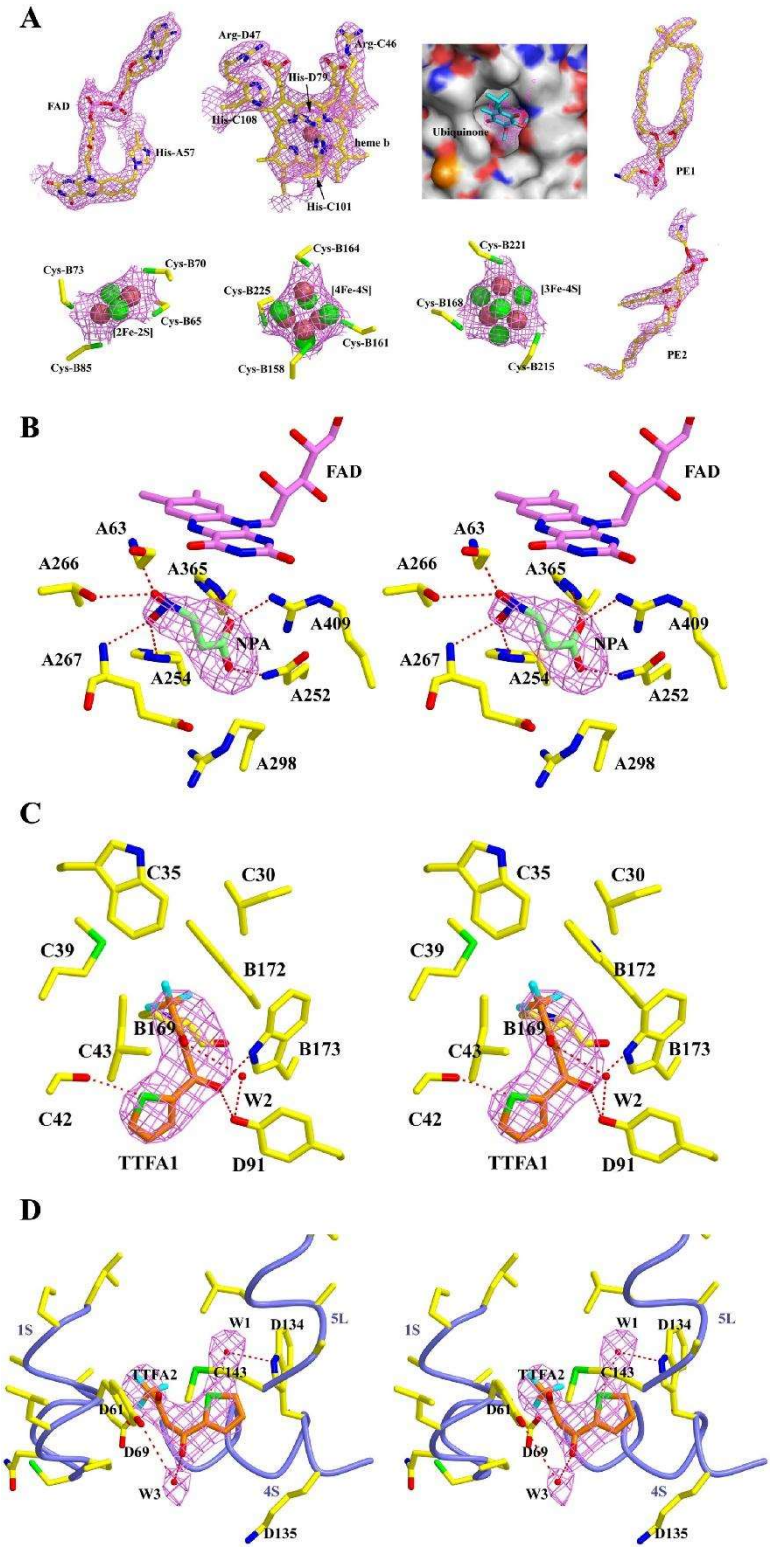

Figure 5. The Mitochondrial Respiratory Complex II Structure with binding inhibitors (Sun *et al*., 2005)

3-nitropropionate (NPA), a succinate analogue which inhibits succinate-oxidation enzymatic activity. NPA molecules are shown (Figure 5B) to be found near a Flavin mononucleotide group of FAD. Due to the electron density at the Succinate binding site, it suggests NPA interacts with the side chains A266 and His-A254 of the nitryl group. As well as the main chains of Glu-A267 and Gly-A63 and the FMN group of FAD. The amide group of Gln-A252 anchors the carboxyl group one side while the guanidinium group of Arg-A409 and the imidazole group of His-A365 anchor the other side (Sun *et al.*, 2005).

The role of Complex II in the virulence of human fungal pathogens is not well understood and for this reason its inhibition needs further exploration as a possible antifungal therapy. It already has promising signs that the function of Complex II is linked to morphogenesis. A study showed inhibition of quinone reduction activity with TTFA was shown to completely inhibit filamentation in *C. albicans* (Watanabe *et al.*, 2006).

1.6.2.2 Lonidamine mechanisms of actions

The mechanism of action that LND utilises is the same as seen by TTFA (Figure 5C and 5D). When LND was administered succinate levels increased and Fumarate levels decreased. LND and NPA in combination induced a two-fold increase in succinate levels of the SDH enzyme (Guo *et al.*, 2016). When TTFA was used in combination with LND, TTFA treatment resulted in a larger increase of succinate accumulation. This suggests both LND and TTFA act in the

quinone reduction activity by occupying its ubiquinone binding sites. It is shown (Figure 5C and 5D) that TTFA molecules are found in the proximity of [3Fe-4S] and at the distal side of the transmembrane anchor, potentially the same as LND. As both drug molecules compete with each other's binding sites, increasing doses of LND inhibition of SQR activity was found to be much greater than inhibition of SDH activity at all LND concentrations tested (Guo *et al.*, 2016). This could suggest that LND failed to fully block the electron transfer from the Iron-sulfur cluster to PMS (Phenazine Methosulfate) and MTT (artificial electron acceptors) that allow for a redirection past Ubiquinone. This provides further evidence that LND seems to inhibit complex II activity by the same mechanisms of TTFA which are the interference of the ubiquinone reduction site.

An article in 1988 stated that Lonidamine had ~70% inhibition of mitochondrially bound hexokinase and aerobic glycolysis in Ehrlich ascites tumor cells (FLORIDI *et al.*, 1988). In a more recent paper in 2015, the mechanisms of Lonidamine were highlighted in detail. The report states that a significant amount of succinate is accumulated in LND-treated cells. LND inhibits the formation of fumarate and malate and suppressed succinate-induced respiration of isolated mitochondria. LND also inhibits the succinate-ubiquinone reductase activity of respiratory complex II without fully blocking succinate dehydrogenase activity. LND also induced cellular reactive oxygen species through complex II. The ability of LND to promote cell death was potentiated by its suppression of the pentose phosphate pathway, which resulted in inhibition of NADPH and

glutathione generation. LND also increased glutaminolysis but decreased reductive carboxylation of glutamine-derived α-ketoglutarate (Guo *et al.*, 2016).

Very recently, LND which is a tumor-selective inhibitor of oxidative phosphorylation was modified into a Mito-LND form (Mitochondria targeting). The Mito-LND form showed to be 100-fold more potent than the original form. It inhibited mitochondrial bioenergetics in lung cell viability, growth progression and metastasis in mice (Cheng *et al.*, 2019). Mito-LND caused no toxicity in mice even when administered for 8 weeks up to 50 times the effective inhibitory dose (Cheng *et al.,* 2019).

Malonate is known to be an inhibitor of the SDH enzyme and as it cannot be metabolised, this could act as a competitive inhibitor for complex II inhibition (Wojtovich,A.P *et al.* 2013).

During the 1960's complex II inhibitors were used in agriculture but due to their toxicity in mammalian cells, they cannot be utilised in the healthcare sector so LND could potentially be a solution.

1.6.3 Complex III and complex IV

Complex III and IV inhibitors are readily available, but most are too toxic for mammalian cells. An example of toxicity is Antimycin A which is a very potent complex III inhibitor. Human cells upon administration of Antimycin A have shown loss of cellular viability, mitochondrial structure and function, and

autophagy activity. It has been observed that antimycin A evoked dose-dependent cell death, a rapid loss in mitochondrial membrane potential, and a collapse of oxidative phosphorylation (Hytti, M*. et al*. 2019). Complex III inhibition leads to G0/G1 arrest through redox alteration-mediated DNA damage response and regresses glioblastoma multiforme (*in vivo* mice model) as already shown by the novel mitochondrial complex-III inhibitor Mahanine (Bhattacharya, K. *et al.* 2014).

Inhibition of mitochondrial complex IV has shown to affect succinate-cytochrome *c* reductase which leads to secondary loss of complex II-III activity in the ETC (Hargreaves, I. P. *et al*. 2007). Cyanide is a potent complex IV inhibitor but use pharmacologically is hindered by the acute cyanide toxicity being attributed to inhibition of cytochrome c oxidase (CcOX), the oxygen-reducing component of mitochondrial electron transport (Leavesley, H. B. *et al*. 2008).

A paper published in 2019 (Yamashita *et al.*, 2019) showed the novel arylamadine T-2307 exhibited in vitro antifungal properties against pathogens. T-2307 inhibited respiration of yeast cell isolates in a dose-dependent manner. Complexes III and IV were inhibited in both *S. cerevisiae* and *C. albicans* so this would suggest that the T-2307 would act similarly with *C. glabrata.* It also suggested that T-2307 has little effect on bovine respiratory complexes (Yamashita *et al.*, 2019) so this would be promising for furthering on to clinical trials.

1.7 Aim of study

The role of complex II inhibitors such as TTFA has been well established but the need for a less toxic alternative which can be used safely in mammalian cells is needed. The aim of this study is to see if LND has significant anti-fungal properties on *C. glabrata* clinical isolates. It will be measured against comparative potent complex II inhibitor TTFA alongside a closely related comparative species *S. cerevisiae* due to the wide array of laboratory strains available. The specific objectives of the anti-fungal analysis will be LND's effect on SDH activity, cell viability, growth cycle and biofilm formation. Once examined, the discussion will aim to investigate any potential mechanisms of *C. glabrata* to compensate with treatment of LND.

2. Materials and Methods

2.1 Drug concentrations

LND (MW 321.2g/mol) was prepared by adding 2mL of DMSO (>99.7% assay percent range) to a vial of 50mg LND to produce a final concentration of 77.8mM. The LND final concentration was aliquoted into 200µL aliquots and stored in -10^{o}C. Tocris were the supplier used when ordering LND.

TTFA (MW 222.18g/mol) was prepared by adding 10mL of ethanol (>99% assay percent range) to a 25mL falcon tube containing 333.27mg TTFA to produce a final concentration of 150mM. The TTFA final concentration was aliquoted into 1mL aliquots and stored in -10^{o}C. If possible, it is advisable to prepare and use solutions on the same day. Upon opening of a vial, allow the vial of TTFA to equilibrate to room temperature for at least 1 hour. Thermo Fisher Scientific were the supplier used when ordering TTFA.

2.2 Analysis of yeast cell growth

2.2.1 Growth curve assay

5mL YPD medium was placed into each test tube that is required and using an inoculation loop, the loop was passed through a Bunsen burner to ensure that the loop is sterile. Once cooled, the inoculating loop was passed through a

colony of a maintenance plate and placed into the 5mL YPD medium. This was repeated for each strain required. All test tubes were placed on a rotary shaker at 180 RPM at a temperature of 30ºC. Approximately 14-18 hours later, OD_{600} 0.2 of overnight culture of each strain was placed into 1mL of sterile RPMI 1640 media in each well of a Greiner 24 well plate (RPMI media to be used to ensure conditions replicate the physiological conditions of glucose levels in mammalian blood rather than nutritionally rich media such as YPD). 778 μM LND, 0.5mM - 1.5mM TTFA, 1% DMSO and 1% ethanol were pipetted into the necessary wells. Triplicate repeats were prepared along with a contamination control (RPMI only). The 24 well plate was measured for 24 hours (TTFA) or 40 hours (LND) using a BMG LabTech SPECTROstar nano plate reader (Table 1). Analysis of growth curve data was analysed by using the MARS software.

Table 1. Measurement settings on the BMG LabTech SPECTROstar nano.

Excitation	600nm
Cycle time	360 seconds
Shaking frequency	400 RPM
Shaking Mode	8-minute linear shake followed by double orbital shaking
Temperature	30°C
Positioning Delay	0.5 seconds

2.2.2 Doubling times (Td) ½

Using growth curve data from MARS software, exponential growth rates were then calculated in Excel using the log of the number of cells at time (t) minus the

log of the number of cells at time zero (t_0), which equals the growth rate constant multiplied by the time interval: $\mu = ((\log_{10} N - \log_{10} N_0) 2.303) / (t - t_0)$.

2.3 Tetrazolium blue chloride (BT) assay

For analysis of Succinate dehydrogenase activity of *C. glabrata* with complex II inhibitors TTFA and LND, the reagent Tetrazolium blue chloride is an appropriate assay. The BT assay measures cell proliferation by reduction of the tetrazolium salt, BT (3,3′-(3,3′-Dimethoxy[1,1′-biphenyl]-4,4′-diyl)-bis(2,5-diphenyl-2H-tetrazolium) dichloride). This tetrazolium salt produces a blue coloration in the cells as they form a formazan product via succinate dehydrogenase.

Overnight culture of *CG2509* cells used in the experiment were cultivated in 5mL YPD medium at 30^{o}C on a rotary shaker at 180 RPM for 24 hours. 0.1 OD_{600} of *CG2509* was pipetted into 3 Eppendorf tubes and labelled ‘WT’, ‘778µM LND’ and ‘1.5mM TTFA’. All tubes were centrifuged at 11600 x g for 2 minutes and the supernatant removed. 1mL of RPMI-1640 medium was added to each Eppendorf tube and the pellet was resuspended after vortexing to ensure the cell pellet was completely resuspended. 1.5mM TTFA and 778µM LND were pipetted into their designated wells and a 1mL of cell free control medium containing RPMI-1640 was prepared alongside. All 4 Eppendorf tubes were incubated at 22^{o}c for 90 minutes. The cells (500µl) were mixed with 250µl of 25mg/mL Tetrazolium blue chloride (BT) and incubated for 2 hours at 30^{o}c.

To each Eppendorf tube, 500µl of Propan-2-ol containing 0.04 HCl was added and the solution was vortexed at the highest speed (10) for 2 minutes. The acidity ensured that the cell walls lyse and the BT-formazan which is contained with the cells were released into the solution. Each Eppendorf tube was then centrifuged at 11600 x g for 2 minutes to allow for the cells to form a pellet at the bottom of the tube and for the dye to remain in the supernatant. The supernatant was pipetted into a 96-well plate and the absorbance of the supernatants were measured at 570nm wavelength against a cell-free RPMI-1640 medium control.

2.4 Cell viability assay

The strain *CG2509* was grown in YPD overnight under standard growth conditions. A serial dilution of the overnight culture was performed and cells were counted under microscopy until ~2000 cells were present in 10µL of culture. 10µL of culture was then pipetted onto fresh YPD plates in technical triplicates of the following conditions: YPD (WT control), YPD+ 1mM TTFA, YPD+ 778µM LND, YPD + 1% DMSO (solvent control) and YPD + 1% ethanol (solvent control). After 72 hours hours of incubation at 30ºC, colony formation was counted via microscopy.

2.5 Respirometry

2.5.1 Respiration profiles of *C. glabrata* clinical isolates

The determination of oxygen consumption and capacity of each *C. glabrata* clinical isolate was performed using an O2k Oxygraph (Oroboros) high resolution respirometer in order to first get a respiratory profile. A 2ml suspension of the cells grown in YPD overnight containing approximately 1 million cells per mL was transferred into both chambers. A 20-minute period of cellular routine respiration was allowed to reflect the metabolic activity under cell culture conditions. 8µl of 50mM Triethyltin Bromide (TET) was added to each chamber resulting in the leak of respiration caused by compensation for the proton leak after inhibition of ATP synthase. Following the leak 2µl of 12mM FCCP (mitochondrial oxidative phosphorylation uncoupler) was added to each chamber to uncouple the electron transport chain from the oxidative phosphorylation system through interference of the proton gradient. Finally, 2µl of 20mM Antimycin A was added to each chamber inhibiting respiration through inhibition of complex I and II of the electron transport system.

2.5.2 Respiration profile of *C. glabrata* with LND titration

The determination of oxygen consumption and capacity of each *C. glabrata* clinical isolate was performed using an O2k Oxygraph (Oroboros) high resolution respirometer in order to first get a respiratory profile. A 2ml suspension of the cells grown in YPD overnight containing approximately 1 million cells per mL was transferred into both chambers. A 20-minute period of

cellular routine respiration was allowed to reflect the metabolic activity under cell culture conditions. 10µl titrations of LND were added (0.389mM to final concentration of 2.723mM) once the trace of the graph had begun to plateau. Finally, 2µl of 20mM Antimycin A was added to each chamber to inhibit respiration through inhibition of complex I and II of the electron transport system in order to measure NMR.

2.5.3 Respiration profile of *C. glabrata* with Flavone and LND titrations

The determination of oxygen consumption and capacity of each *C. glabrata* clinical isolate was performed using an O2k Oxygraph (Oroboros) high resolution respirometer in order to first get a respiratory profile. A 2ml suspension of the cells grown in YPD overnight containing approximately 1 million cells per mL was transferred into both chambers. A 20-minute period of cellular routine respiration was allowed to reflect the metabolic activity under cell culture conditions. 1 titration of 10µM Flavone was added and 3 further titrations of LND (0.389mM to final concentration of 1.167mM) once the trace of the graph had begun to plateau. Finally, 2µl of 20mM Antimycin A was added to each chamber inhibiting respiration through inhibition of complex I and II of the electron transport system in order to measure NMR.

2.6 Crystal violet staining analysis of *C. glabrata* biofilm

2.6.1 Growing the biofilm

Overnight culture of *CG2509* cells used in the experiment were cultivated in 5mL YPD medium at 30ºC on a rotary shaker at 180 RPM for 24 hours. 100µL of the overnight culture was added to each well in a 96 well plate. Wells were prepared in technical triplicates with the following conditions: YPD (cell free control), YPD + 1mM TTFA, YPD + 778µM LND, YPD + 1% DMSO (solvent control) and YPD + 1% ethanol (solvent control). The 96 well plate was incubated for 48 hours at 37ºC.

2.6.2 Staining the biofilm

To note, crystal violet is toxic and stains very strongly so ensure goggles, gloves and laboratory coats are worn at all times when staining with CV.

After incubation, cells were discarded by turning and shaking out the YPD medium. The plate was submerged carefully into a tub of water and gently shaken. This was repeated for a second time. Shaking allowed for removal of cells which were not attached and also for remaining medium that may have been background staining to be kept to a minimum. 125µL of a 0.1% solution of crystal violet was added to each well of the 96 well plate. The 96 well plate was incubated at room temperature for 15 minutes. The plate was rinsed 4 times with water by submerging as before in a tub of water and shaking carefully. Once the plate had been rinsed 4 times, the plate was blotted on a stack of

paper towels to remove any excess dye. The plate was turned upside down and allow to dry for 24 hours.

2.6.3 Quantifying the biofilm

125μL of 30% acetic acid was added in water to each well of the 96 well plate to ensure the CV solubilized. The plate was incubated at room temperature for 15 minutes. 125μL of the solubilized CV was transferred to a new 96 well plate and the absorbance values were read in a plate reader at 550nm. The 30% acetic acid in water was used as a control.

2.7 Flow cytometry analysis of Cellular H2O2 production

3mL overnights were inoculated to OD600 0.1 and incubated with the fluorescent indicator dye H2DCF-DA (final concentration 5 μg/ml) for 24 hours in a SpectroStar plate reader. ROS production was analysed in triplicate, with an additional culture per strain acting as an undyed control. Cells were grown in a plate reader to measure their growth and ensure that all strains had undergone diauxic shift. After 24h of growth, 2.5μl of each culture was suspended in 500μl PBS (pH 7.4), stained with propidium iodide (PI; final concentration 2 μg/ml), and assessed for ROS production using a BD Accuri™ C6 Plus flow cytometer. 10000 cells per sample were analysed. Cells were classified into one of four groups using a PI-only WT positive control heated for 5 min at 80^{o}C (Figure 6.). The proportion of high ROS cells reported corresponds to the proportion of cells in the lower right quadrant of Figure 6.

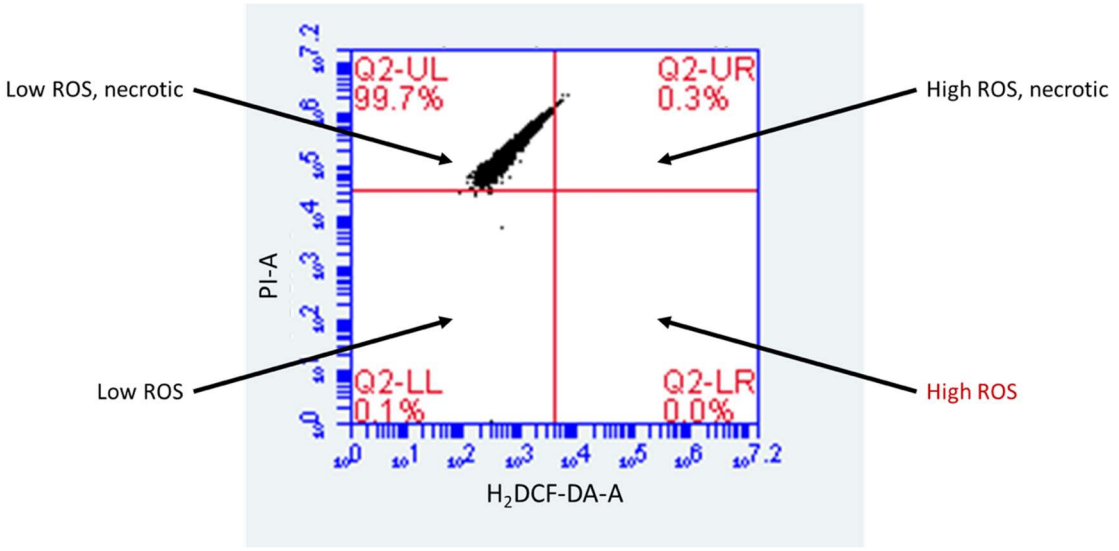

Figure 6. Classification of cell types according to H2DCF-DA and PI signal characteristics. Cells were classified using a quadrant placed around a positive control group of WT cells dyed with PI and heated at 80°C. Cells with a PI signal greater than the lowest signal observed in the positive control were classified as necrotic, and those with a H2DCF-DA signal greater than the highest signal observed in the group were classified as high ROS.

2.8 Preparing transformants for lacZ reporter assays

2.8.1 Preparation of the plasmid transformation for the *S. cerevisiae* TCA mutants

This protocol allowed for the insertion of plasmids to express CIT2-lacZ tagged proteins within the *S. cerevisiae* strains used in this study. Cells were grown overnight in YPD under standard growth conditions. 400µl of the cell culture was pipetted into an Eppendorf tube and incubated at 30°C for 4 hours to ensure the cells are in log phase. Cells were centrifuged at 4000 RPM for 5 minutes. The supernatant was removed from the pellet, which was then washed and resuspended in 400µL of sterile water. 100µL of the suspension was transferred into Eppendorf tubes and labelled as controls and strains with the CIT2-lacZ

plasmid. The Eppendorf tubes were then centrifuged at 4000RPM for 30 seconds and the supernatant was removed. Into each of the Eppendorf tubes, 360μl of the master mix (prepared by the ingredient list shown in table 2).

Table 2. The reagent list to prepare a master mix

Reagents	**1 transformation**
PEG 3500 50% w/v	240μL
LiAc 1.0 M	36μL
Boiled SS-carrier DNA	10μL + 40μL sterile water
Plasmid DNA	5μL + 29μL sterile water
Total	360μL

The cells were bathed in a water bath for 40 minutes at 42^{o}C then centrifuged at 10000RPM for 30 seconds and the supernatant was removed. The cells were re-suspended in 200μL of sterile water. The cells were plated on the necessary selective plates (SD-URA agar plates) and incubated at room 30^{o}C for 3-5 days, then checked for colony growth to assess successful transformation.

2.8.2 *BY4741* strains used for transforming with CIT2-lacZ plasmid

Table 3. *S. cerevisiae* strains used from the BY4741 mutant library

ORF name	Gene
YER065C	ICL1
YNL117W	MLS1
YPR001W	CIT3
YLR304C	ACO1
YOR136W	IDH2
YIL125W	KGD1
YOR142W	LSC1
YGR244C	LSC2
YPL262W	FUM1
YLL041C	SDH2
YKL085W	MDH1

2.9 β-galactosidase liquid culture assay

Cells transformed with a lacZ plasmid were grown in SD-URA overnight and then sub cultured to OD_{600} 0.1. Triplicate replicates were prepared with the following conditions: 778μM LND, no drug and no cells (control). All of the cells were allowed to grow to for 24 hours. In microcentrifuge tubes. 100μL of culture was added to 500μL of Z buffer (reagent list as seen in table 4) and incubated at 30°C for 30 minutes. 150μL of ONPG solution was added and then shaken by

hand to start the reaction. After 12 hours, 400μL of 1.5M Na_2CO_3 was added to halt the reaction. Samples were centrifuged for 1 minute at 10,000RPM and the absorbance measured at 420nm and 550nm.

Table 4. Ingredient list for Z-buffer and ONPG

Reagent	Description
Z buffer	60mM Na_2HPO_4, 40mM NaH_2PO_4, 10mM KCl, 1mM Mg_2SO_4, 50mM β-merceaptoethanol (added directly before use before use.)
ONPG	4mg/ml dissolved in water (prepared and used in one day due to sensitivity to light).

2.10 PyMoL analysis of the LSC2 beta subunit

2.10.1 Screening species for fungal specific residues in LSC2

The origin sequence of the beta subunit LSC2 was gathered from the most common fungal species from the NCBI protein database (https://www.ncbi.nlm.nih.gov/protein/) along with the equivalent found in *H. sapiens* and *M. Musculus*. Sequences were compared using Clustal Omega Multiple Sequence Alignment (https://www.ebi.ac.uk/Tools/msa/clustalo/).

2.10.2 iTasser structural predictions of LSC2

From the origin sequence gathered from the NCBI protein bank in section 2.10.1, the sequences were uploaded to the iTasser online service provided by the Zhang lab (https://zhanglab.ccmb.med.umich.edu/I-TASSER/annotation/) and a predicted structure of the LSC2 enzyme for both *S. cerevisiae* and *H. sapiens* were generated. The PyMoL predicted structure files (.pdb) were downloaded.

2.10.3 Visualising the fungal specific region on LSC2 with PyMoL

By using PyMoL software, it was made possible to overlay the predicted structural LSC2 enzymes by opening both .pdb files in PyMoL. The fungal specific tyrosine was highlighted red by utilsing the sequence mode. The residue site was found by entering sequence mode, right clicking the Tryosine and clicking the colour palette. The structures were overlayed by clicking display and then clicking overlay.

2.10.4 Modifying the fungal specific region on LSC with PyMoL

By zooming into the fungal specific region on PyMoL and selecting the region, the default ribbon structure was changed to stick form view. By selecting the residue and entering builder mode, the Tyrosine was replaced with different amino acids as seen in section 4.8.

3. Results

The project sought to investigate and compare the respiration characterisitcs in both a series of clinical isolates of the human fungal pathogen *C. glabrata* and *S.cerevisiae* laboratory strains. In addition, a series of assays were conducted to determine the effects of inhibition of SDH in both *C. glabrata* and *S. cerevisiae*. It was examined whether SHD inhibition, or loss of TCA or glyoxylate cycle functionality, led to respiratory stress and reduced viability. These experiments were aimed to increase our understanding as to whether SDH and mitochondrial metabolism are suitable targets for anti-fungal drug development.

3.1 The effects of LND addition on *C. glabrata* growth

Growth assays were performed over a period of 40 hours comparing control and LND treated cells. Treatment with DMSO (solvent control) led to inhibition of *C. glabrata* growth (Figure 7B) that was also observed in LND treated cells (Figure 7A). However LND treatment led to pronounced cell aggregation as seen in the widening and eratic nature of the curve during (Figure 7A). The aggregation was observed in all isolates (Figure 7 ia representative graph, see appendix 1 for the other *C. glabrata* clinical isolate growth curves).

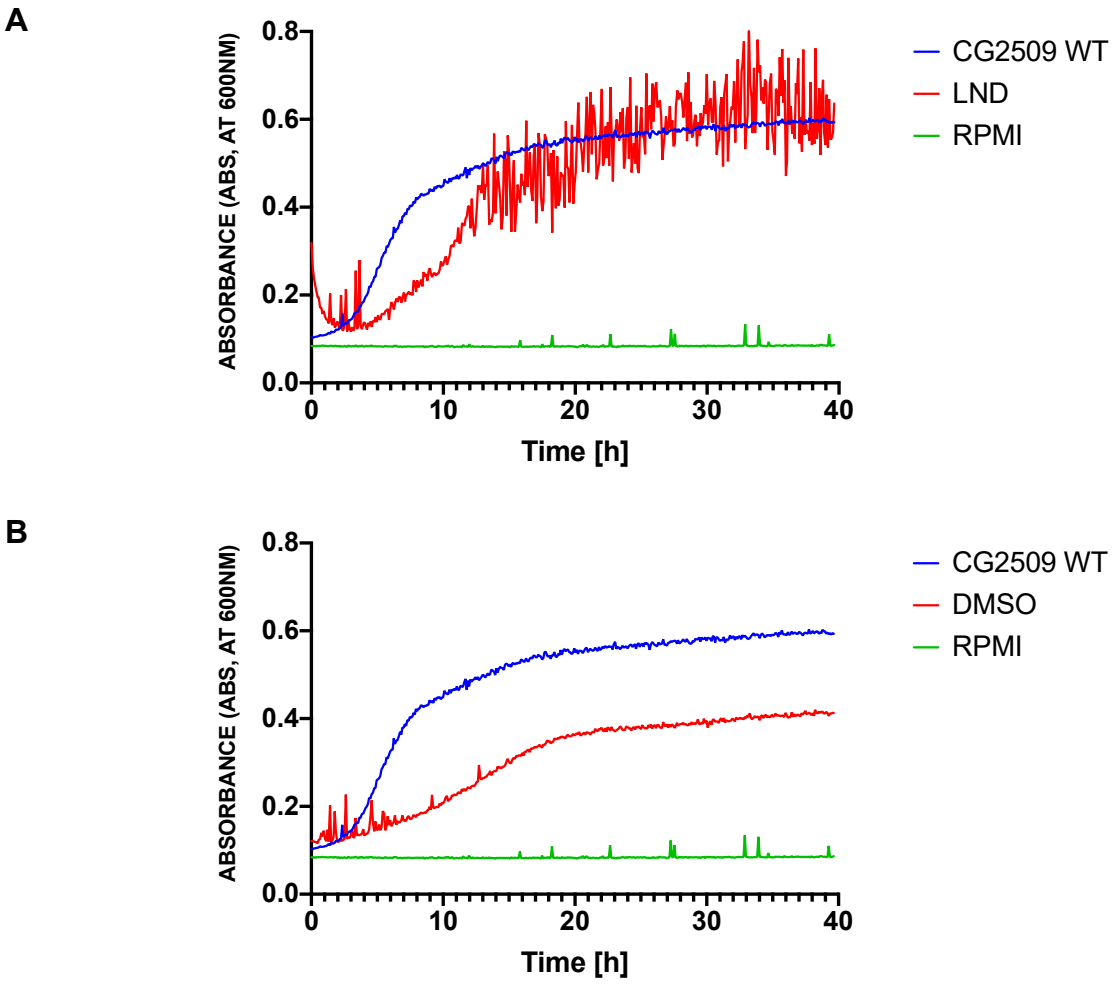

Figure 7. Growth assay of *C. glabrata* clinical isolate with 778 μM LND and 1% DMSO in RPMI media over 40 hours. (A) Clinical isolate *CG2509* growth comparison with LND treated cells. (B) Clinical isolate *CG2509* growth comparison with DMSO treated cells.

To complete the growth analysis, doubling times were calculated for all four clinical isolates when with LND treated cells compared to WT control cultures containing the solvent (Figure 8). LND treatment led to a significant increase in doubling time in three out of the four clinical isolates, with the fourth showing a similar trend. These data confirm that LND treatment leads to growth inhibition.

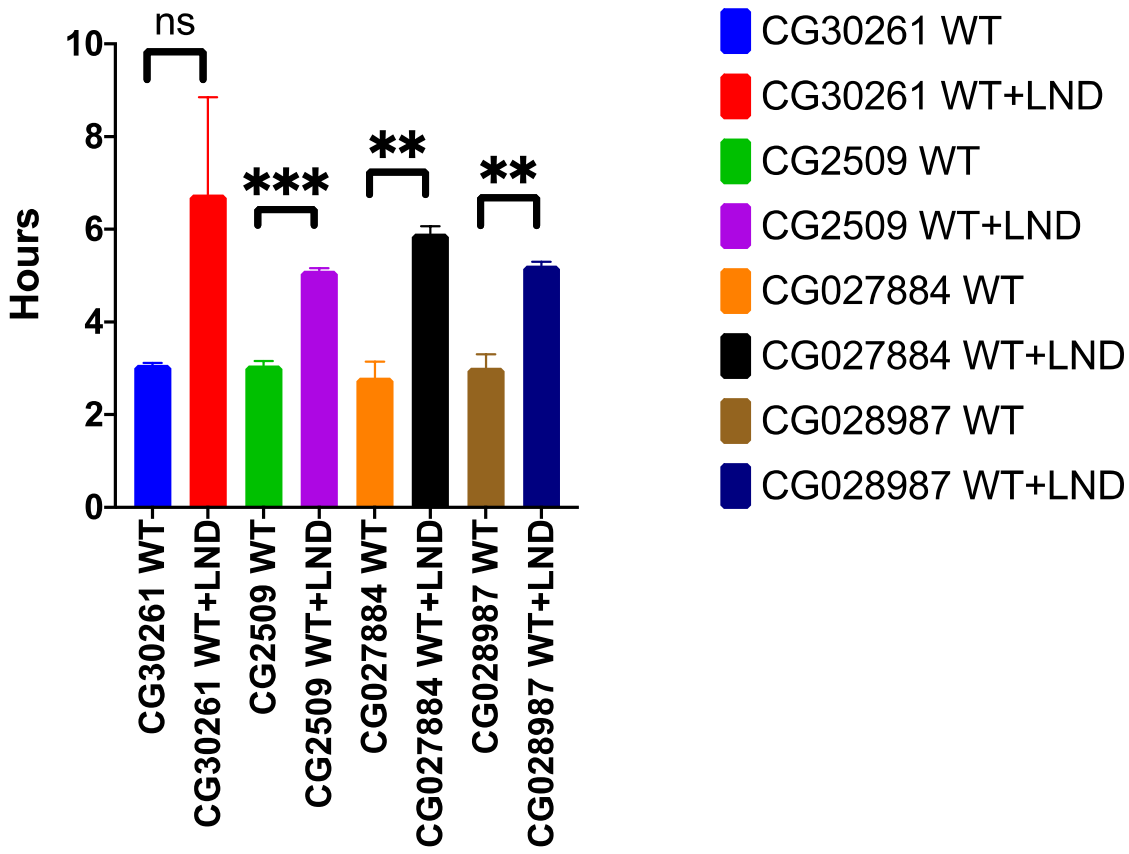

Figure 8. Doubling times of *C. glabrata* clinical isolates were measured and represent the slowing effects of LND on the cells ability to grow during exponential phase. The statistical analysis of the doubling times for *CG30261* were non significant, *CG2509 (P < 0.005), CG027884* (*P < 0.05)* and *CG028987 (P<0.05)*.

3.2 Effects of TTFA on *C. glabrata* growth

Having assessed the effects of LND treatment on *C. glabrata,* it led to testing whether similar effects were observed in the presences of the potent complex II inhibitor TTFA. TTFA also led to inhibitory effects on the growth of *C.glabrata* (Figure 9A) at all three concentrations. The ethanol solvent control confirmed that ethanol alone was not causing this reduction in growth (Figure 9B). Representative graphs are presented. Together these data sets suggest that SDH inhibition leads to growth inhibition in *C. glabrata* clinical isolates.

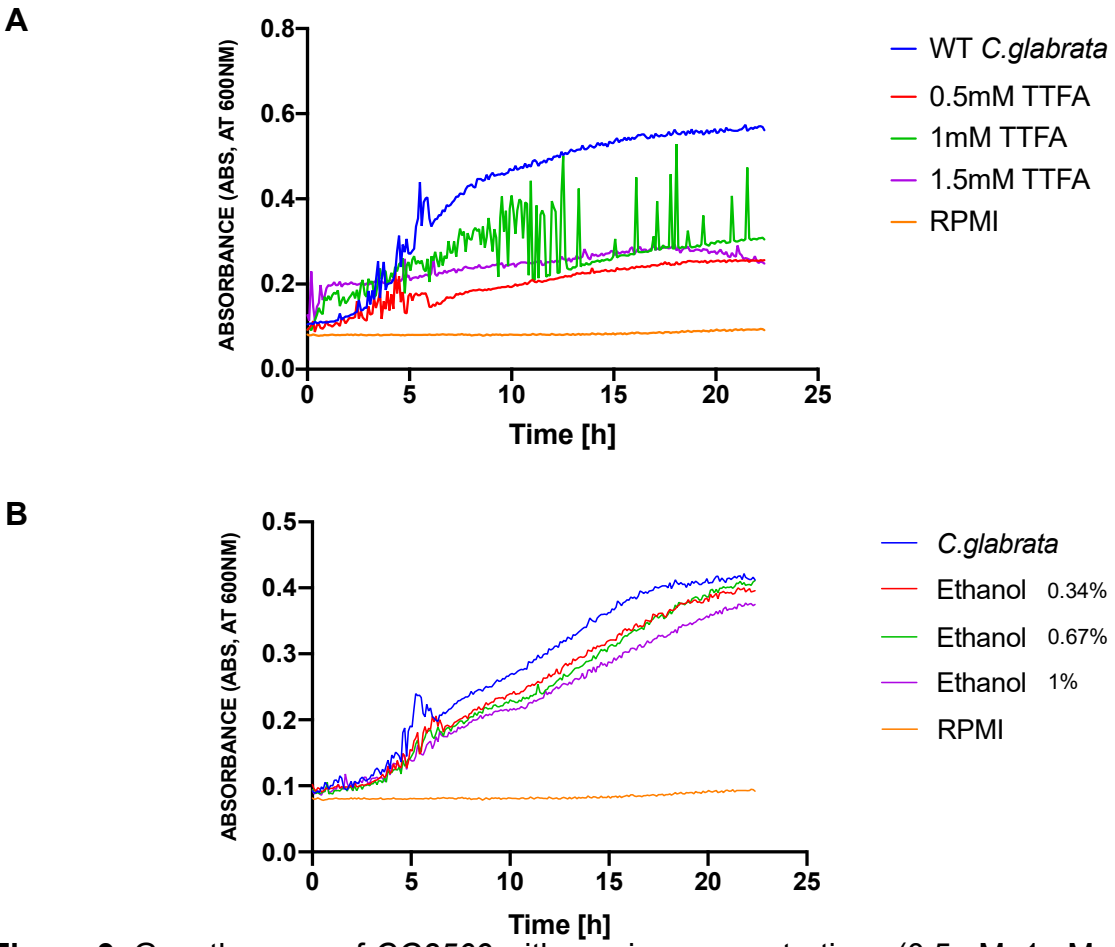

Figure 9. Growth assay of *CG2509* with varying concentrations (0.5mM, 1mM and 1.5mM) of TTFA and upto 1% ethanol in RPMI media over 24 hours. (A) WT growth comparison with TTFA treated cells. (B) WT growth comparison with ethanol treated cells.

3.3 Effects of LND treatment on SDH activity in *C. glabrata*

Having seen that LND had a significant effect on *C. glabrata* clinical isolates, it was important to determine if the drug was inhibiting SDH activity. This can be achieved by assaying reduction of the tetrazolium salt Nitroblue tetrazolium (BT) and observing production an insoluble product that can be measured at an OD of 570nm using a spectrophotometer. The experiment confirmed that exposure of *C. glabrata* cells to either LND or the well characterised SDH inhibitor

prevented BT reduction (Figure 10). This suggests that LND acts as an SHD inhibitor in *C. glabrata*.

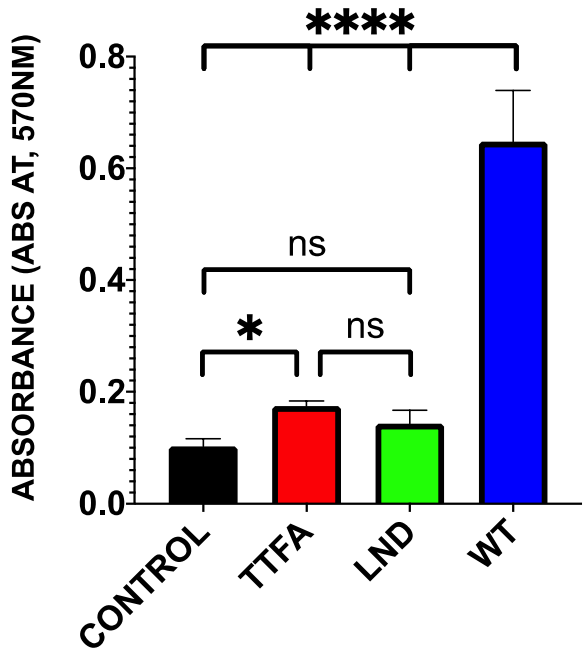

Figure 10. The strain *CG2509* was grown in YPD overnight under standard growth conditions along then inoculated to OD_{600} 0.1 with technical triplicates of YPD, YPD+ 1mM TTFA and YPD+ 778μM LND. After 24 hours, NBT was added to each to measure the reduction of the tetrazolium salt. The reaction was halted and absorbance value were taken at OD 570nm using a spectrophometer. The BT asborbance value represent inhibitory effects of TTFA and LND on the ability of *C. glabrata* to proliferate by measurement of the reduction of tetrazolium salt.

3.4 Effects of SDH inhibition on *C. glabrata* viability

After confirmation that LND was indeed inhibiting the SDH enzyme on par with the highly potent complex II inhibitor (TTFA), it led to determining whether inhibition of SHD activity led to a reduction in viability in *C. glabrata* clinical isolates. To achieve this, the data suggests that inhibition of SDH with either LND or TTFA led to a reduction in cell viability relative to their solvent controls (Figure 11).

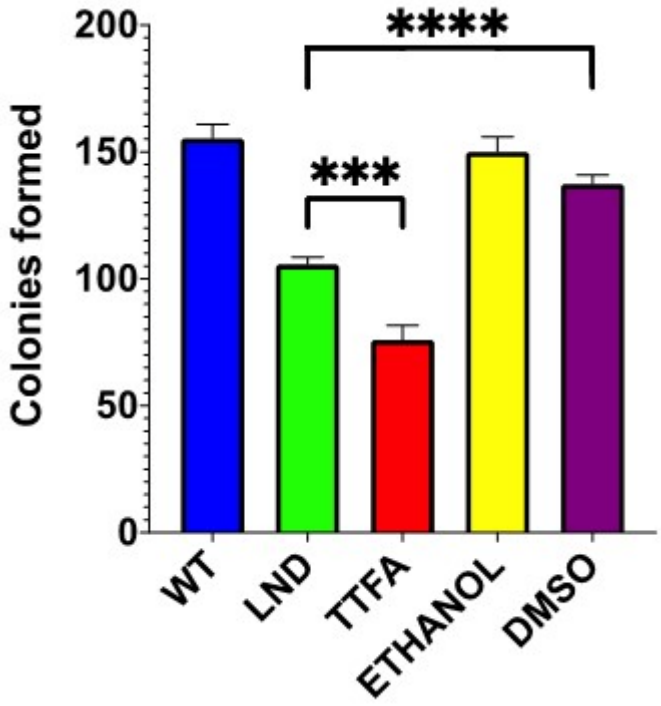

Figure 11. The strain *CG2509* was grown in YPD overnight under standard growth conditions. A serial dilution of the overnight culture was performed until ~2000 cells were pipetted onto YPD plates in technical triplicates of the following conditions: YPD (WT control), YPD+ 1mM TTFA, YPD+ 778μM LND, YPD + 1% DMSO (solvent control) and YPD + 1% ethanol (solvent control). After 72 hours hours of incubation, colony formation was counted via microscopy. Inhibitory effects of TTFA and LND on the ability of C. glabrata to produce viable colonies on a YPD petri dish over 4 incubating days. One-way anova analysis was performed (****P<0.005*, *****P<0.0005*).

3.5 Effects of SHD inhibition on Respiration in *C. glabrata* clinical isolates

3.5.1 Respiratory profiles of the *C. glabrata* clinical isolates

In order to measure how the respiration of the *C. glabrata* clinical isolates coped with LND treatment, a high resolution respirometer was used. Initially, it was

crucial to characterise *C. glabrata* respiratory profiles in each of the four clinical isolates.

In order to gather the data the following protocol was performed. Routine respiration was obtained before the introduction of the ATPase inhibitor triethyltin bromide (TET) which induces a build up of protons within the into the membrane space and inhibition or respiration linked to ATP produciton. Oxygen consumption that occurs following TET application requires non-ATP synthase associated proton movement across the inner mitochondrial membrane and is referred to as LEAK respiration. The difference between LEAK and routine respiration suggested how coupled ATP synthesis is linked to the ETC. FCCP acts as an uncoupler by making pores in the membrane, in a reversible manner, allowing protons to flow through the pore. This caused a dissipation of the membrane potential which in turn allows maximum movement of electrons through the ETC. Measurement following FCCP addition therefore referred to the maximum respiration potential. This maximum value provides an insight into just how fast this electron transport chain may go and to what extent it is suppressed. Following FCCP addition, a measurement was then taken after introduction of the irreversible Complex III inhibitor Antimycin A. Inhibition of complex III stops electrons flowing through the chain past complex III and prevents all mitochondrial associated oxygen consumption. The difference between routine and the value after adding Antimycin A shows what level of oxygen consumption due to mitochondrial respiration. Any residual oxygen consumption following Antimycin addition represented non-mitochondria O_2 consumption. A large value by non-mitochondria O_2 consumptions may occur if

cells have upregulated other oxygen consuming processes such as fatty acid beta oxidation in the peroxisomal compartment. By producing respiratory profiles for all four clinical isolates, it highlighted how much variance there is amongst clinical isolates. The routine respiration for *CG027884* (Figure 12B) is abnormally high along with the leak (proton) respiration compared to the other clinical isolates despite all isolates sharing similar MAX (maximum respiration). All isolates produce NMR once Antimycin A impaired the mitochondrial function. As the respiratory profiles were not statistically analysed, it can be not said that this fluctuation across the isolates happened by chance. For future work, it would be beneficial to repeat. Having generated the respiratory profiles, it allowed for respiratory experiments on LND treated cells to see if LND has an effect on NMR once complex II is inhibited or whether *C. glabrata* can overcome mitochondrial disruption by LND.

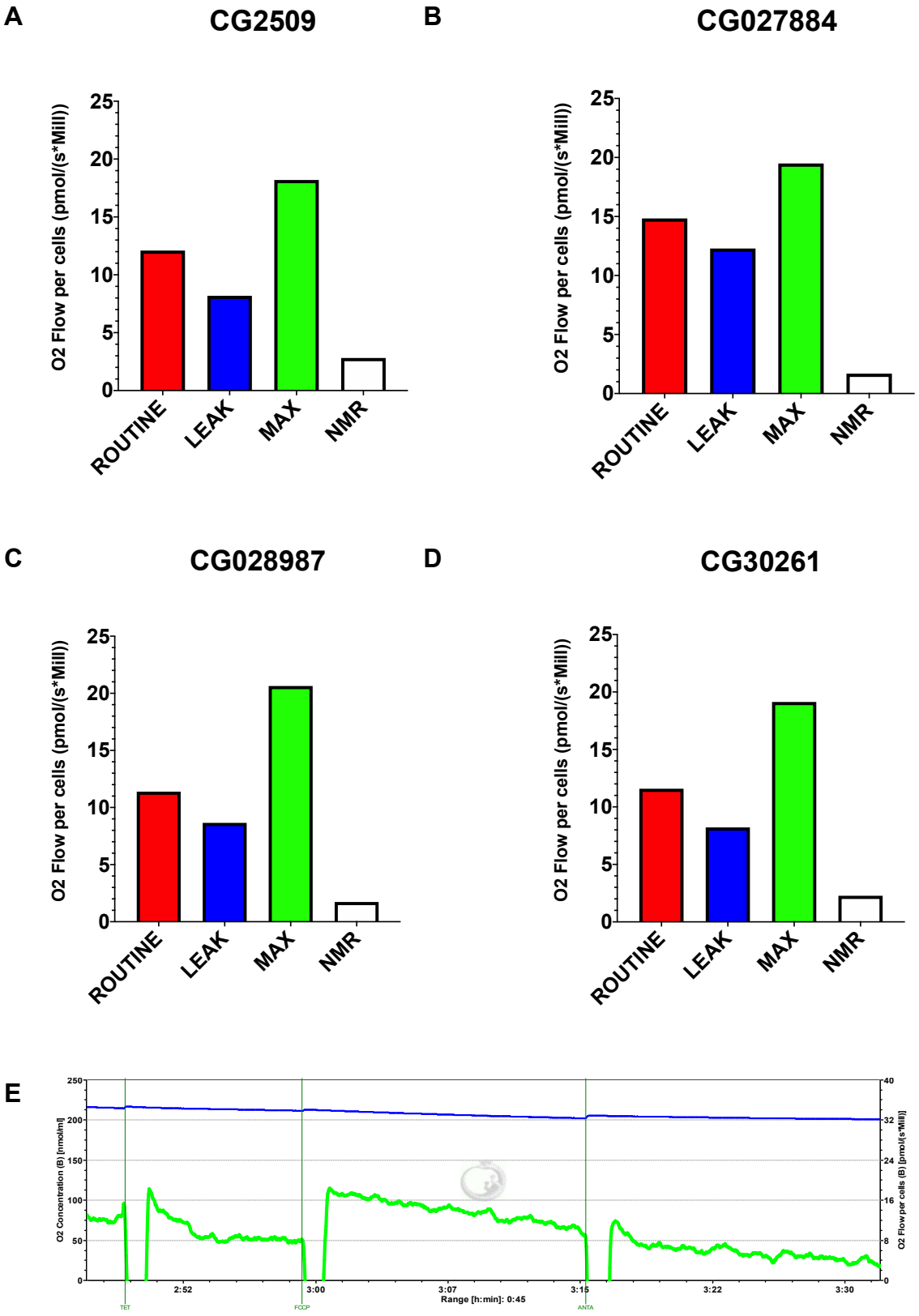

Figure 12. Respirometry profiles of overnight cultures (grown for 18 hours) of *C. glabrata* clinical isolates during stationary phase. Cells were left to reach a stable ROUTINE before adding 50mM TET to represent the LEAK, 12mM FCCP was added to represent to represent the MAX and 20mM Antimycin A was

added to represent the NMR. (A-D) Bar graphs show the similarity of all isolates respiratry profile whereby all have a routine which is slightly higher than the LEAK. All four show the highest value in the MAX and a very small NMR. (E) *CG2509* is shown an example of a respirometry profile taken in DataLab.

3.5.2 Effects of LND on the *C. glabrata* respiration

The respirometry analysis of *C. glabrata* LND was performed in order to see if loss of SDH activity would lead to respiratory failure. Into the respirometers chambers of 2mL YPD, ~1 million cells per mL were added to each chamber after using a cell counter to dilute the overnight culture accordingly. Cells were left to reach routine before titrating DMSO (0.5% to a final concentration of 3.5%) into chamber A and LND (0.389mM to a final concentration of 2.723mM) into chamber B, titrating again once the traces began to reach routine. The respirometry analysis (Figure 13) shows an initial drop once drug or solvent is added, this is to be considered irrelevant since this only occurring due to the injected liquid and consequently Oxygen into the chamber. The important finding is once the trace returns (after injection of drug/solvent) and overshoots the routine respiration. In the case of LND, the overshooting is larger than that of ethanol which suggests a transient uncoupling (as happens with FCCP in Figure 12 which is represented as MAX). It confidently shows that SDH inhibition doesn't inhibit respiration and that complex II is not being engaged in the electron transport chain. The effects of SDH inhibition on growth and viability are likely to be a result of non-ETC effects on metabolism.

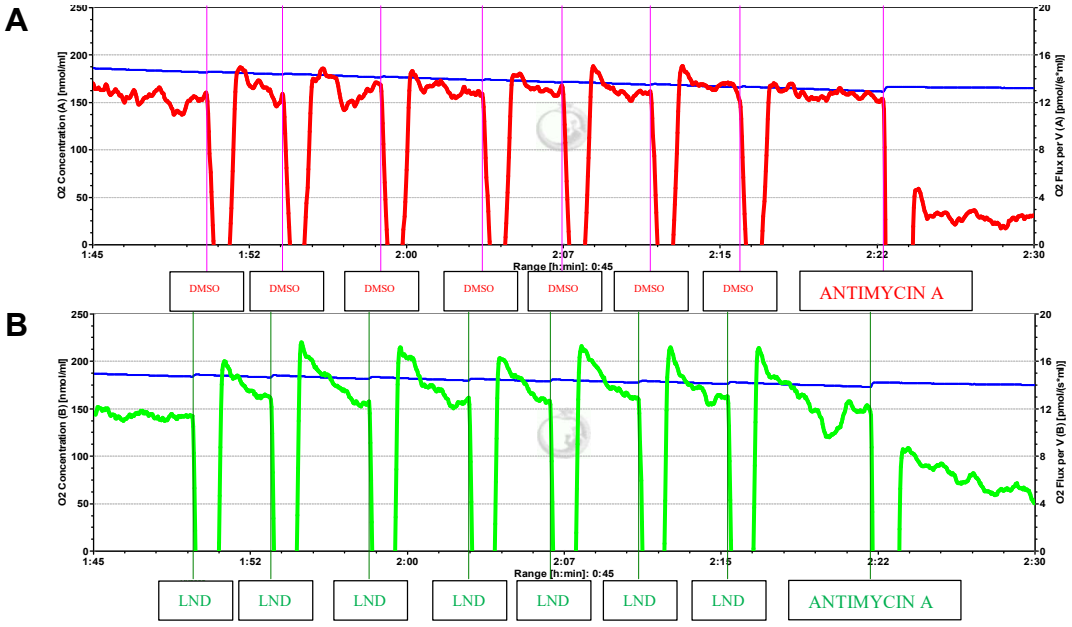

Figure 13. Respirometry DataLab graphs of overnight cultures (grown for 18 hours) of *C. glabrata* during stationary phase. Cells in both chambers were left to reach a stable ROUTINE before adding drugs and solvents. (A) Adding 7 titrations of DMSO (0.5% to a final concentration of 3.5%) as a solvent control. Adding 20mM of Antimycin A reduced mitochondrial respiration completely. Any remaining O2 flux represents NMR. (B) Adding 7 titrations LND (0.389mM to a final concentration of 2.723mM) suggests a transient uncoupling but the cells were able to recover quickly. Finally, adding 20mM of Antimycin A reduced mitochondrial respiration completely. Any remaining O2 flux represents NMR which was higher than that of solvent only.

3.5.3 Effects of NADH dehydrogenase and LND inhibition on *C. glabrata* respiration

C. glabrata does not have a complex I but it does have mitochondrial external NADH dehydrogenase (NDE1 and NDE2) and a NADH Dehydrogenase Internal (NDI1). Flavone, which is a specific inhibitor of the *S. cerevisiae* NDI1 has shown to inhibit almost completely NADH oxidase and NADH-UQ1 reductase activities of NDI1 (Kitajima-Ihara and Yagi, 1998) so was used to test to see if by inhibiting firstly NDI1, that the effects of inhibiting II would amplify the effects of LND. Flavone produced a large peak (Figure 14) which as LND also

produced after administration so suggests further transient uncoupling. The cells were able to overcome the temporary disruptions from both drugs administered. This further suggests that SDH inhibition doesn't inhibit respiration and that complex II is not being engaged in the electron transport chain.

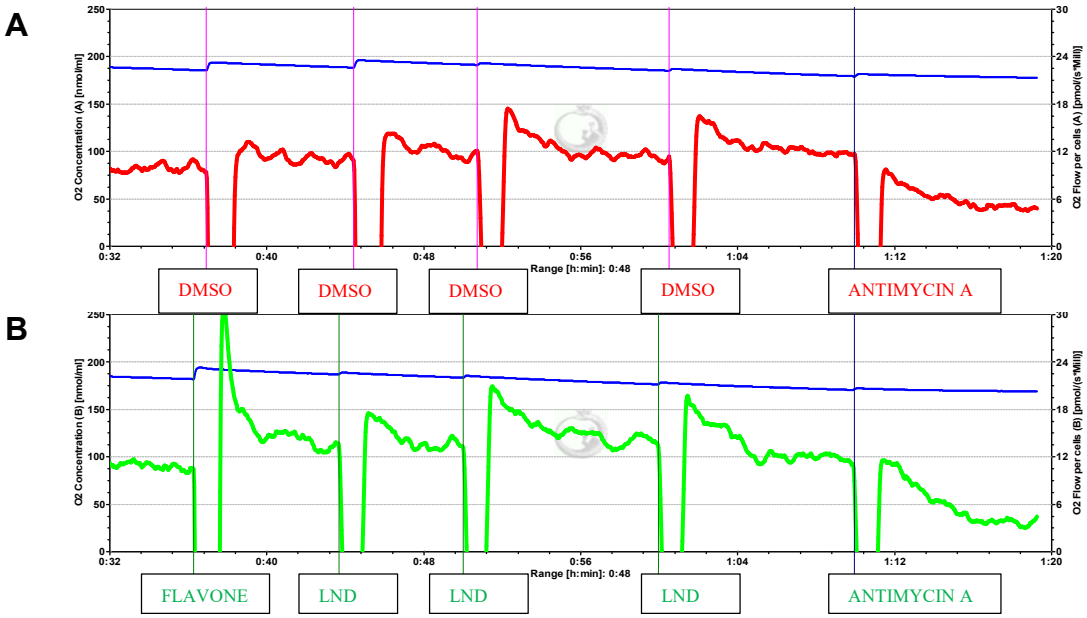

Figure 14. Respirometry DataLab graphs of overnight cultures (grown for 18 hours) of *C. glabrata* during stationary phase. Cells in both chambers were left to reach a stable ROUTINE before adding drugs and solvents. (A) Adding 4 titrations of DMSO (0.5% t to final concentration of 2.0%) as a solvent control showed minor disruptions to the ETC membrane. Finally, adding 20mM of Antimycin A reduced mitochondrial respiration completely. Any remaining O2 flux represents NMR. (B) Adding 1 titration of 10µM Flavone causes a huge membrane disruption and 3 further titrations of LND (0.389mM to final concentration of 1.167mM) caused a transient uncoupling but the cells were able to recover quickly. Finally, adding 20mM of Antimycin A reduced mitochondrial respiration completely.

3.6 Effects of SDH inhibition on *C. glabrata* biofilm formation

C. glabrata cells can form a biofilm and this is a major determinant of its virulence. Biofilms are naturally multi-drug resistant and represent a clinical problem. To determine if inhibition of SDH could inhibit biofilm, overnight culture of *CG2509* were grown for 18 hours. Overnights were diluted to OD_{600} 0.1 in fresh media and 100μL of the culture was placed into a 96 well plate. Triplicate repeats with the following conditions were pipetted: WT control, 1mM TTFA, 778μM LND, 1% DMSO (solvent control) and 1% ethanol (solvent control). After 2 days of incubation (30^{o}C) to allow growth of a biofilm, the mature biofilm was assessed by using crystal violet which stains the biofilm matrix material. It was observed that both TTFA and LND led to a significant reduction in *C. glabrata* biofilm growth. TTFA showed more potent inhibitory effects than LND by reducing the biofilm by ~2/3's ($P < 0.005$) whilst LND reduced biofilm formation by ~1/3 ($P < 0.005$) compared to the wild type (Figure 15).

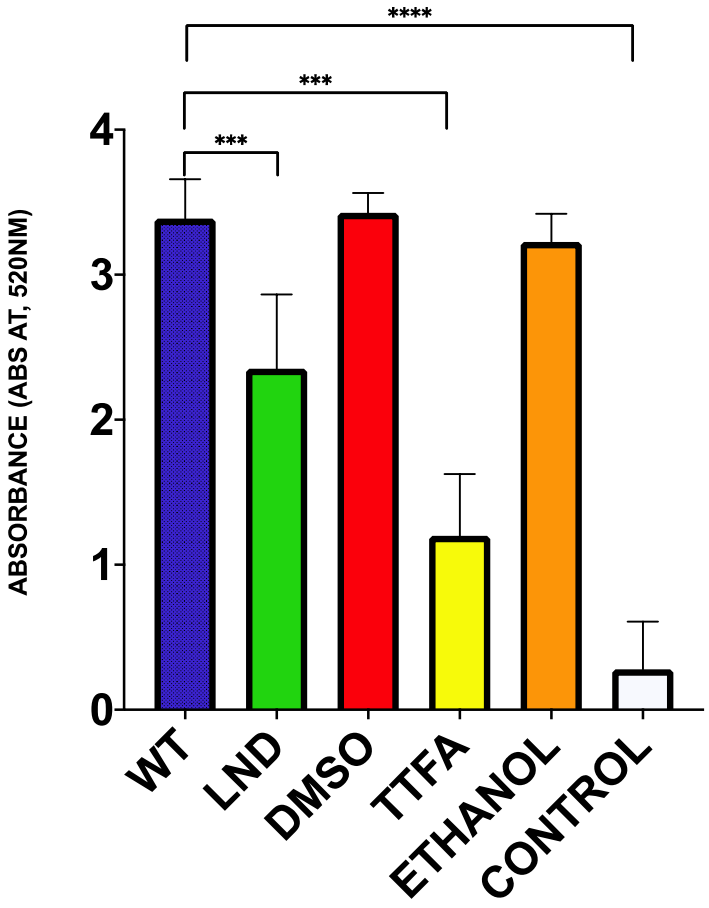

Figure 15. Crystal violet staining representing the inhibitory effects of LND and TTFA on *C. glabrata* biofilm formation at maturity (48 hours at 30ºC). Data is from triplicate repeats with the following conditions were pipetted: WT control, 1mM TTFA, 778μM LND, 1% DMSO (solvent control) and 1% ethanol (solvent control) after 2 days of incubation (30ºC) to allow growth of a biofilm. Error bars based on standard deviation which was calculated from triplicate values (n=3). One-way anova analysis was performed *(***P<0.005, ****P<0.0005)*.

3.7 Effects of SDH inhibition on ROS accumulation

3.7.1 Effects of SDH inhibition on ROS accumulation in *C. glabrata* cells

Flow cytometry analysis of the *C. glabrata* clinical isolates treated with LND was performed to see if ROS accumulated following SDH inhibition. The dye H_2DCFDA is a chemically reduced form of fluorescein used as an indicator for reactive oxygen species (ROS). Upon cleavage of the acetate groups by intracellular esterases and oxidation, the nonfluorescent H_2DCFDA is converted to the highly fluorescent 2',7'-dichlorofluorescein (DCF). Necrotic cells were assessed by the addition of Propidium Iodide (PI). PI is a red-fluorescent cell viability dye which is excluded from live cells with intact membranes but penetrates dead or damaged cells and binds to DNA and RNA by intercalating between the bases. High ROS cells appear in the bottom right quadrant (Figure 16A-C) and high necrotic cells appear in the top left quadrant. PI-A Flow cytometry analysis showed that both the solvent control and LND produced only 0.1% high ROS cells compared to WT. A small increase of 2.4% necrotic cells in LND treated cells compared to WT and this was not from the solvent alone. In the future, it would be crucial to repeat this experiment in order to statistically analyse the data.

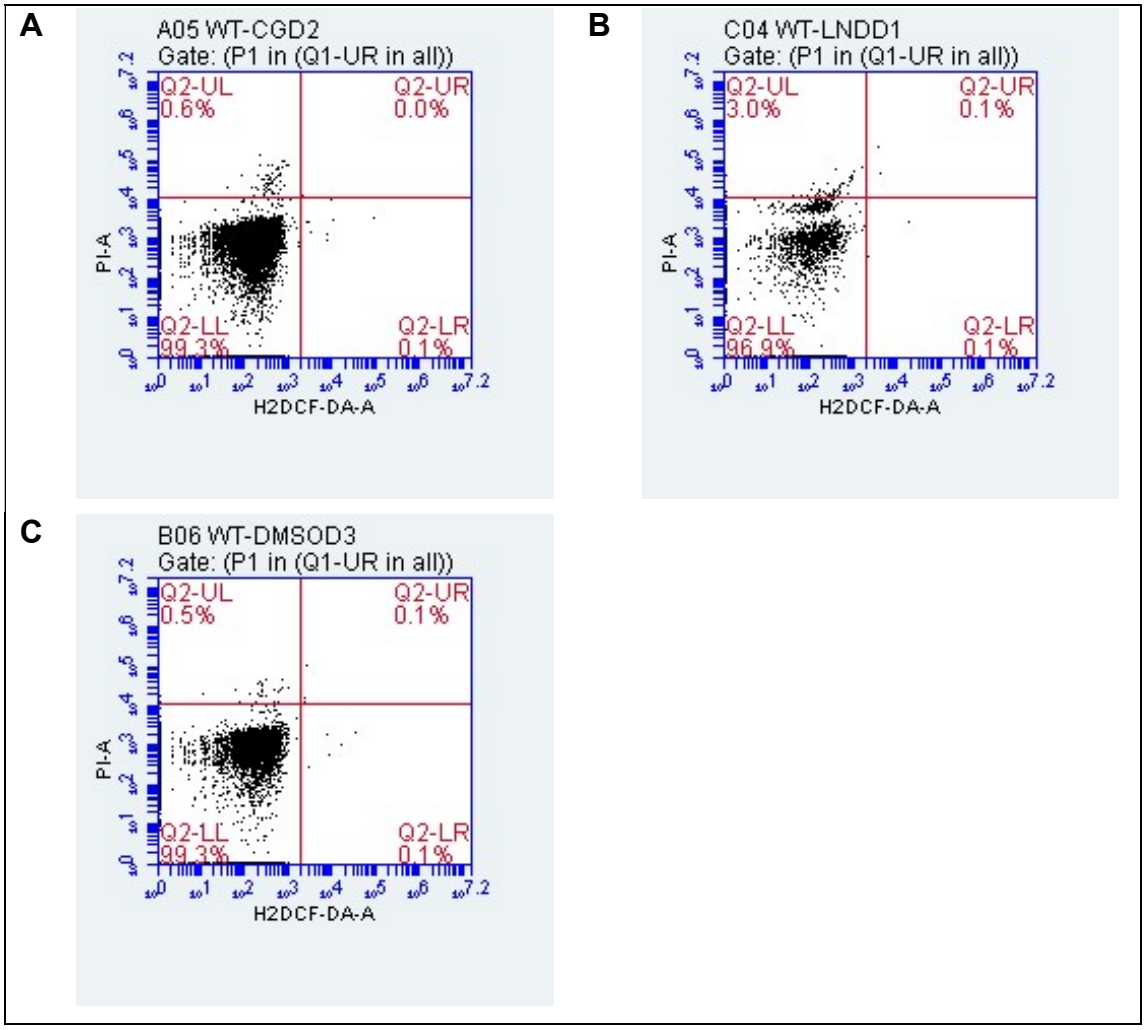

Figure 16. Clinical isolate *CG2509* was grown in glucose overnight, diluted to OD_{600} 0.1 in RPMI and 5mg/mL H_2DCF-DA added except for the control. A 1% DMSO control, a cell free control and a 778μM LND sample was prepared alongside. 2.44mg/mL PI dye was also added which represents necrotic cells. This led to the assessment of both necrosis and ROS production by flow cytometry.Flow cytometry anaylsis showed no difference in levels of ROS production in LND treated *C. glabrata* cells compared to WT. (A) WT (B) LND 0.1 % of ROS (C) DMSO 0.1% of ROS.

3.7.2 Effects of SDH inhibition in TCA and glyoxylate cycle mutant *S. cerevisiae* cells

Having observed that SDH is not operating within the ETC in *C. glabrata*, it was reasoned that it may have stronger effects when applied to cells that are

challenged in TCA and glyoxylate cycles. A list of the most important enzymes involved within both the glyoxylate cycle and the TCA were chosen (Figure 17).

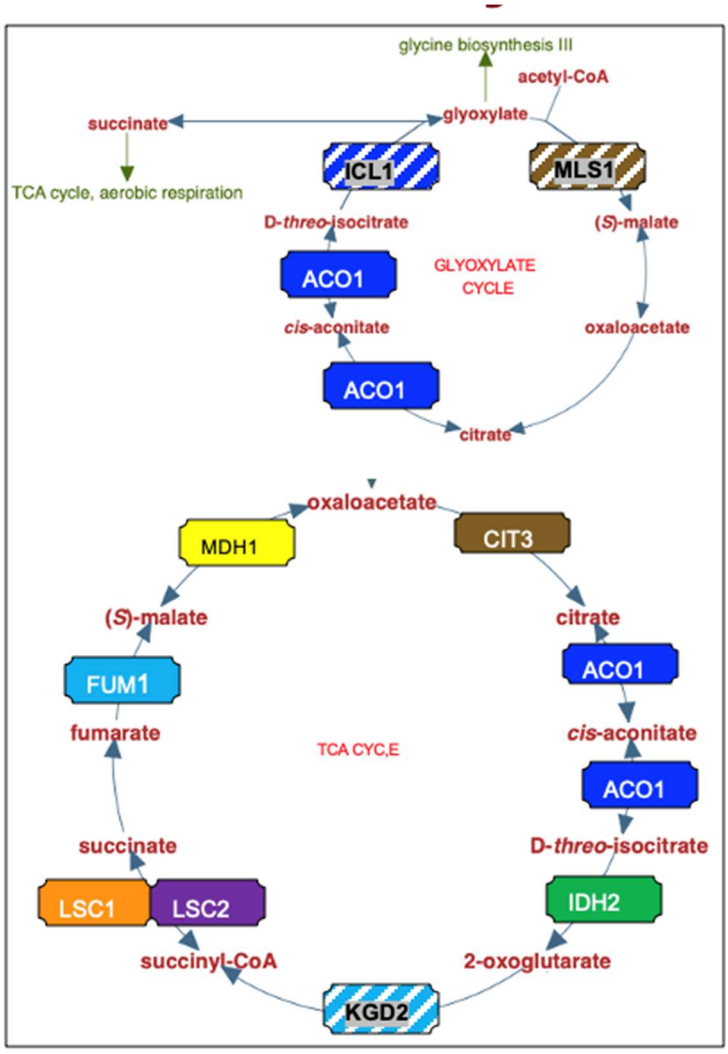

Figure 17. A schematic highlighting the important enzymes involved in each step of the glyoxylate and TCA cycle.

Once the panel of mutants was generated, these were located within the *S. cerevesiae* BY4741 mutant library and streaked out onto fresh YPD plates. The loss of encoded *Δidh2 and Δlsc2*, *Δfum1 and Δmdh1* led to synthetic growth effects when cells were grown in the presence of TTFA. The experiment was only performed once so repeats would be necessary to statistically analyse the

extent of the inhibitory effects. The strains that did not produce produce observable effects were *Δcit1, Δaco1, Δkgd1* and *Δsdh2* (see appendix 2). TTFA treated cells led to a very pronounced effect in stationary phase that may suggest a complete loss of respiration in *S. cerevesiae*.

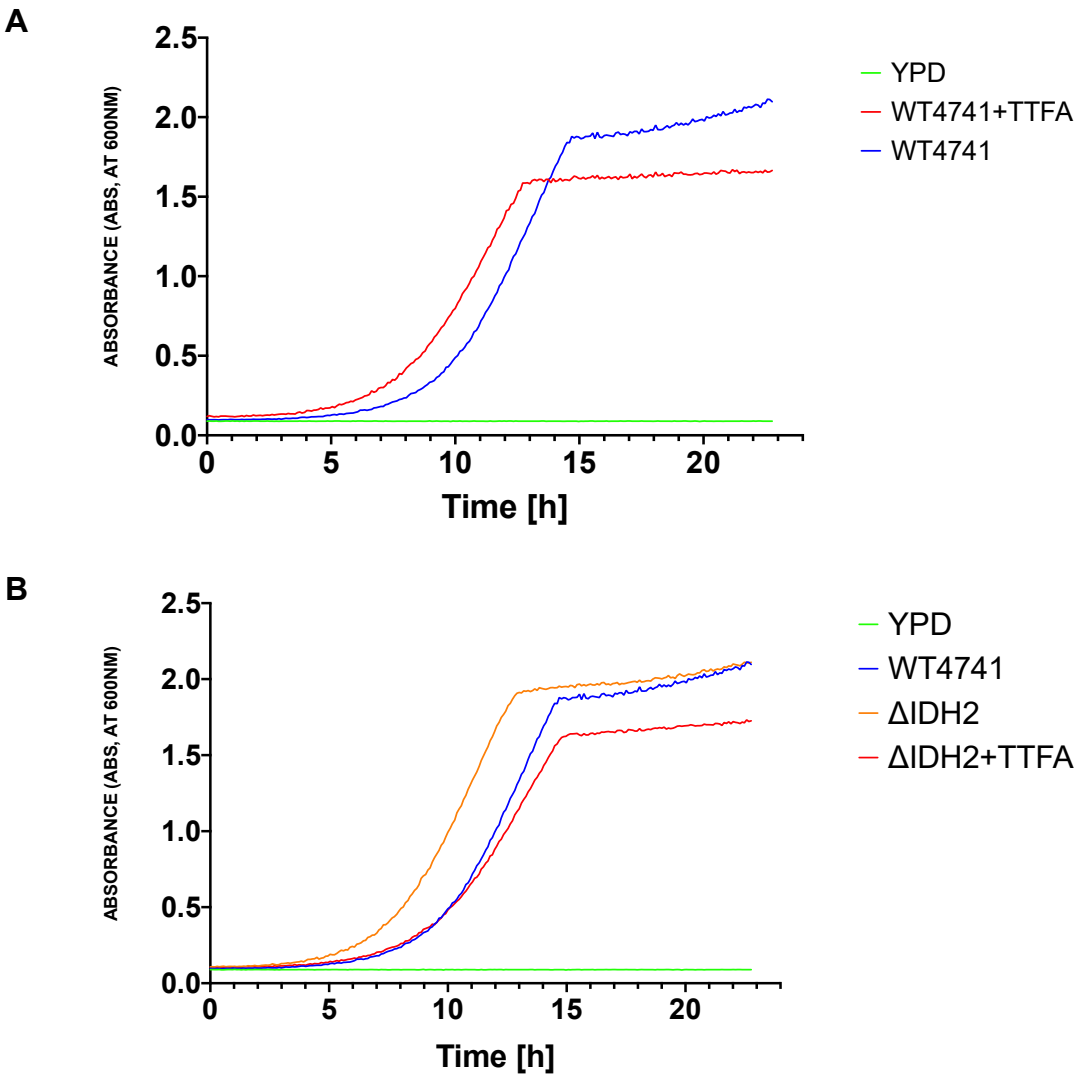

C

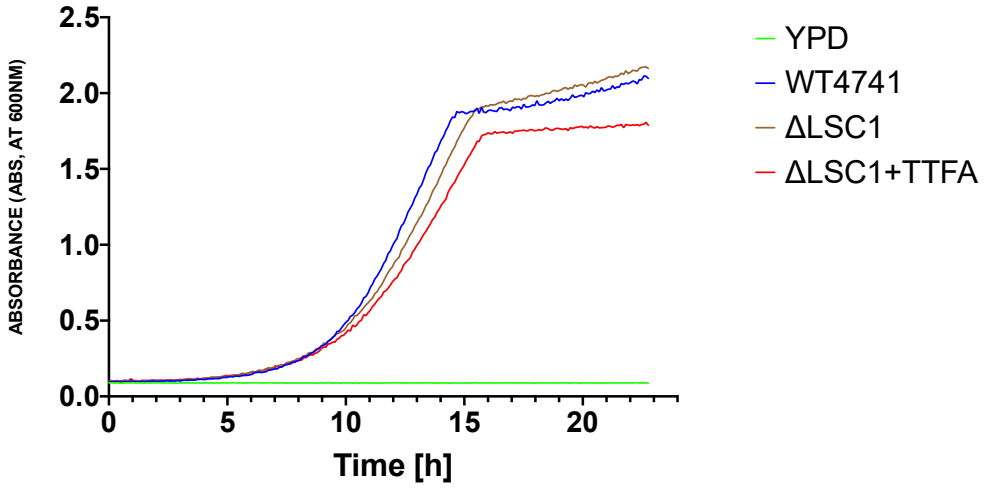
ABSORBANCE (ABS, AT 600NM)
2.5
2.0
1.5
1.0
0.5
0.0
0
5
10
15
20
Time [h]
YPD
WT4741
ΔLSC1
ΔLSC1+TTFA

D

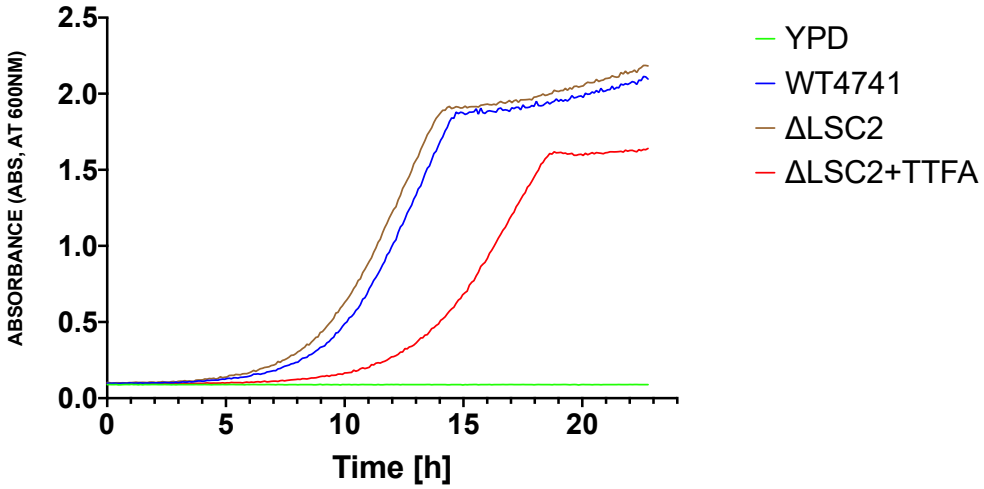
ABSORBANCE (ABS, AT 600NM)
2.5
2.0
1.5
1.0
0.5
0.0
0
5
10
15
20
Time [h]
YPD
WT4741
ΔLSC2
ΔLSC2+TTFA

E

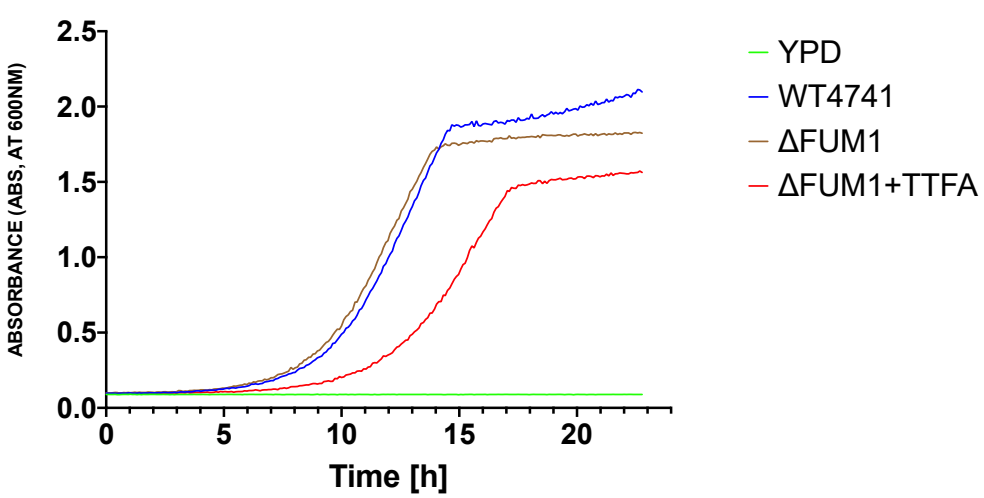
ABSORBANCE (ABS, AT 600NM)
2.5
2.0
1.5
1.0
0.5
0.0
0
5
10
15
20
Time [h]
YPD
WT4741
ΔFUM1
ΔFUM1+TTFA

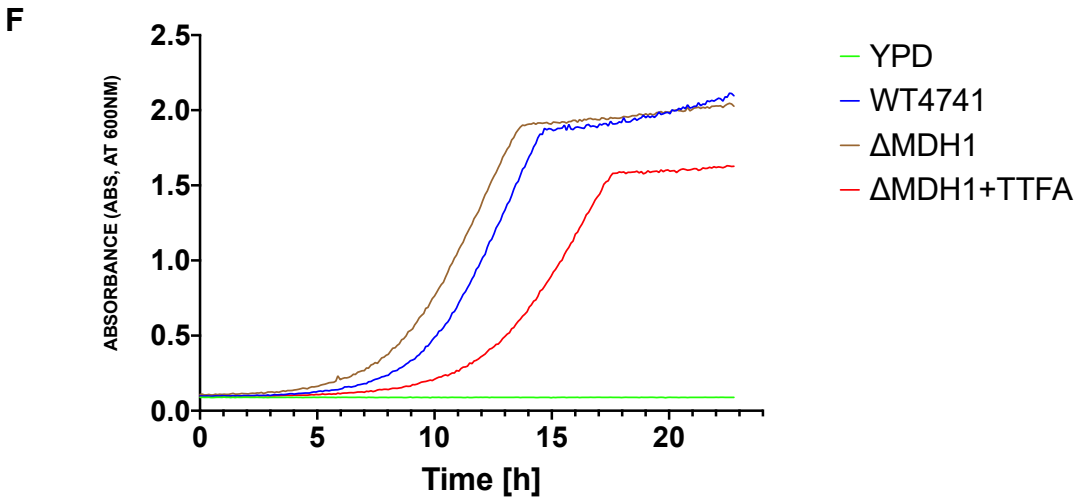

Figure 18. Growth assays of *S. Cerevisiae* which shows loss of respiration during the stationary phase of WT and TCA mutants with 1mM TTFA in YPD media over 24 hours. (A)WT (B)*Δidh2* (C)*Δlsc1* (D)*Δlsc2* (E)*Δfum1* (F)*Δmdh1*.

SDH inhibition does not appear to lead to ROS accumulation in *C. glabrata* cells (Figure 16). This led to investigate whether abrogation of TCA and glyoxylate cycle would lead to ROS accumulation in *S. cerevisiae*. To achieve this, the use of the readily available mutant library was made available. With the loss of SDH activity, it led to experimenting with laboratory strains of *S. cerevisiae* and single TCA knockout mutants which represented each of the major TCA enzymes. Of the enzymes, *Δidh2* and *Δsdh2* were the highest producing ROS mutants. A strain lacking COX4, a core component of complex IV whose loss has been shown to lead to ROS accumulation (Leadsam *et al*., 2014) was used as a positive control.

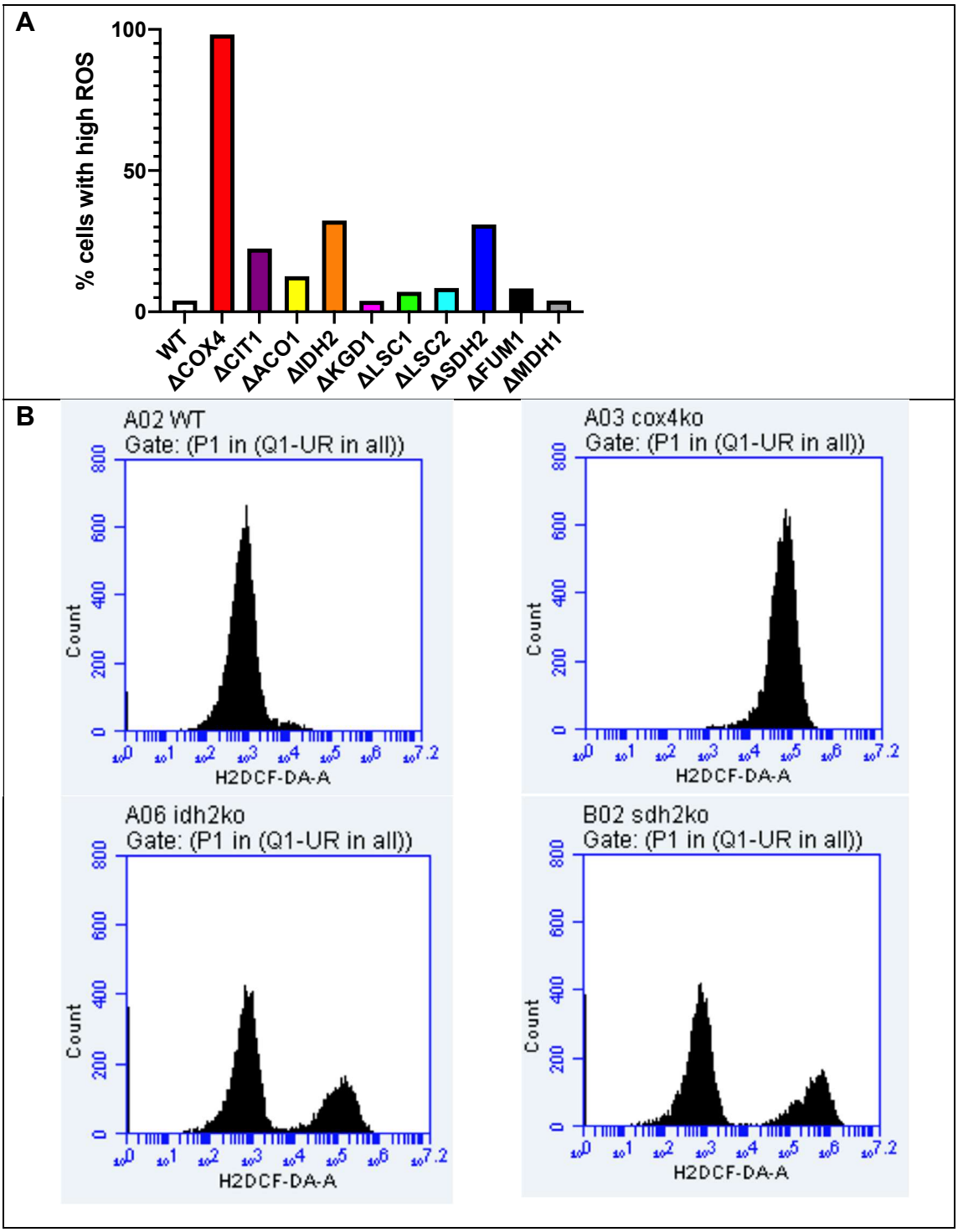

Figure 19. Strains with a single knockout of one of the key TCA enzymes were grown in glucose overnight, diluted to OD600 0.1 in RPMI and 5mg/mL H_2DCF-DA added except for the control. 2.44mg/mL PI dye was also added which represents necrotic cells. This led to the assessment of both necrosis and ROS production by flow cytometry. (A) All of the main TCA enzyme mutants shown in a bar graph whereby *Δsdh2* and *Δidh2* prove to be the biggest ROS producing enzymes. (B)A histogram comparison of WT, Δ*cox4*, *Δidh2* and Δ*sdh2*.

3.8 Linking loss of SDH activity to mitochondrial stress and retrograde signalling

3.8.1 Measuring the effects of LND on the *WT4741* and *⊿sdh2 CIT2* promoter as an indicator of the retrograde signalling

This assay measured *CIT2* levels which is an indicator of retrograde signalling in response to mitochondrial stress. As it is already suggested that SDH inhibition doesn't affect respiration, it led to investigating whether loss of SDH leads to retrograde signalling. The assay showed activation at certain points along the cycle. Having seen how LND was showing anti-fungal properties with cell viability and biofilm reduction but also resisting permanent respiration failure with a dysfunctional mitochondria, it led to seeing if LND was causing an activation of the *CIT2* promoter (indicates an increase in glyoxylate cycle signalling). The ONPG assay showed that LND treated cells ($P < 0.0005$) produced ~4 fold increase in *CIT2* levels compared to WT. It also showed that the *⊿sdh2* gained ($P < 0.0005$) ~2 fold increase in CIT2 levels when administered with LND than that of the *⊿sdh2* with no drug.

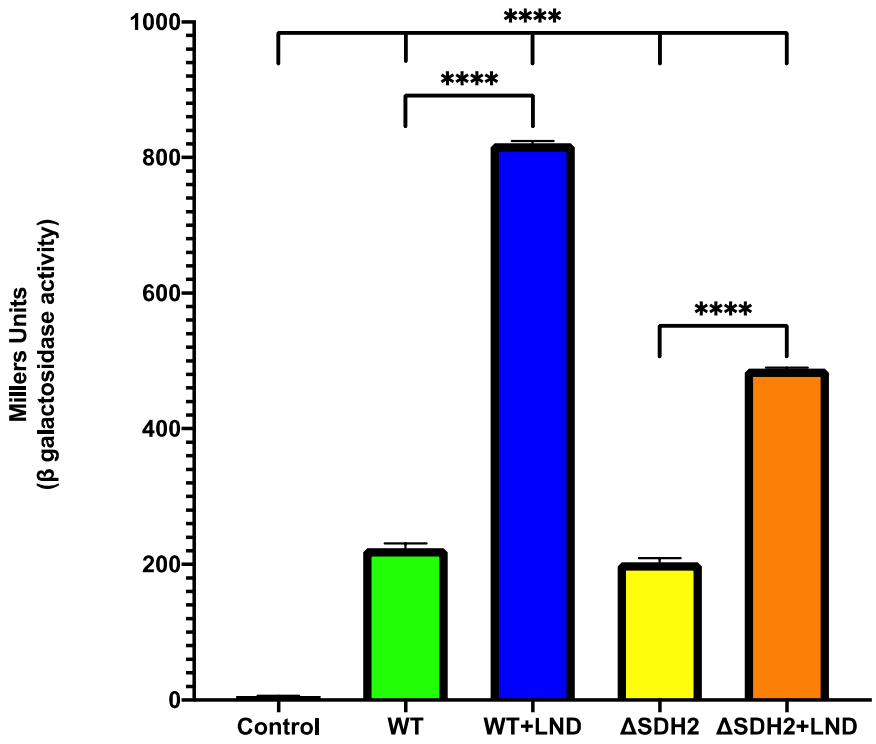

Figure 20. An Overnight culture of *WT4741* and *⊿sdh2* transformed with a lacZ plasmid were grown in SD-URA overnight (in order to preserve the plasmid and ensure cross contamination of species which may thrive in glucose medium) and then sub cultured to OD_{600} 0.1. Triplicate replicates were prepared with the following conditions: 778μM LND, no drug and no cells (control). After a further 24 hours of incubation, the ONPG assay was initiated by addition of ONPG and halted after 24 hours. *CIT2* has served as a prototypical readout for the yeast retrograde response. The ONPG assay allows colorimetric measuring of the activity of the *CIT2* promoter. ONPG provided the substrate for measuring the β-galactosidase activity which is the enzyme encoded by the lac-Z gene, which is being driven by the *CIT2* promoter. This allowed for all the single knockout transformants with a *CIT2*-lacz target to test whether LND was causing an upregulation of the RTG in response to a faulty TCA cycle. ONPG assay comparison of *WT* and *⊿sdh2* when treated with LND for 12 hours. Both *WT* and *⊿sdh2* show a strong correlation between the application of LND and the increase in LacZ activity.

3.8.2 Combinational effects of SDH inhibition and TCA/glyoxylate cycle inhibition on retrograde signalling in *Cerevisiae*

Treatment of *S. cerevisiae* cells with LND led to activation of the CIT2 promoter activity, indicating that retrograde signalling had been activated. This led to see whether this effect would be modulated when TCA and glyoxylate cycles were abrogated. In addition, it was of interest to see whether damage to any

particular steps in the TCA and glyoxylate cycles served as triggers for retrograde signalling. After seeing how LND seemed to sustain activation of the glyoxylate cycle through the elevated CIT2 levels in the ONPG assay (*CIT2* has served as a prototypical readout for the yeast retrograde response), it was worth investigating further to see if there was a specific enzyme in either the TCA or glyoxylate cycle which could show sensitivity to LND. This could lead to future combinational drug therapy. The ONPG assay allowed for all the single knockout transformants with a *CIT2*-lacz target to test whether LND was causing an upregulation of the RTG in response to a faulty TCA cycle. Upon administration of LND, all mutants saw an increase in CIT2 levels except for *Δicl1* (which is located within the glyoxylate cycle). This suggests that ICL1 has an important role within the glyoxylate cycle and ultimately without it, the cells would not be able to synthesis the necessary intermediates by utilising other carbon sources. In the future, it would be crucial to repeat this experiment to in order to statistically analyse the data.

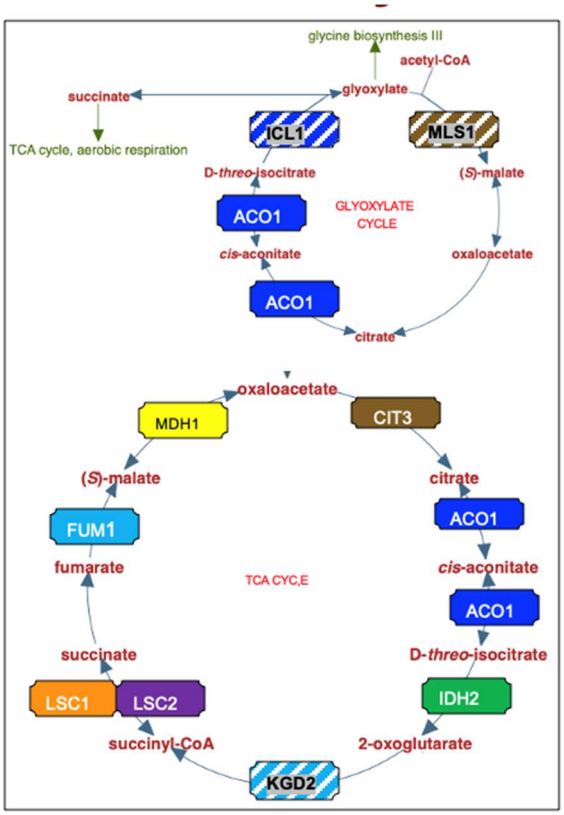

Figure 21. A schematic highlighting the important enzymes involved in each step of the glyoxylate and TCA cycle.

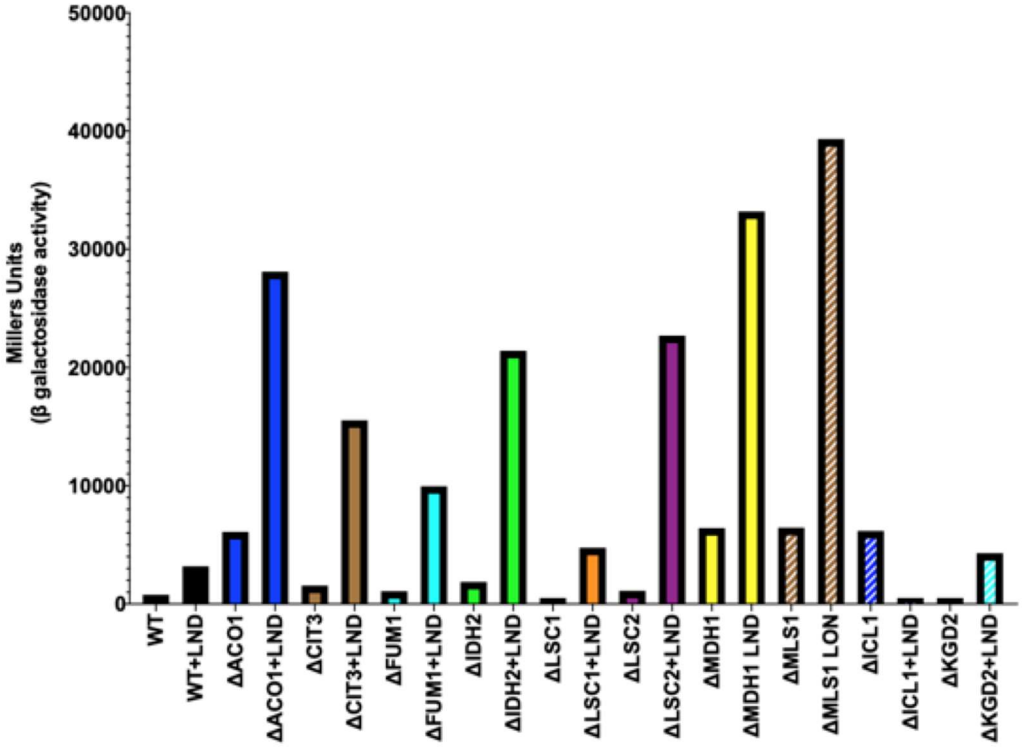

Figure 22. An extended ONPG assay comparison of WT and mutants of the glyoxylate and TCA cycle when treated with 778μM LND for 12 hours.

4. Discussion

Further importance of Succinylation to this project is that it can bring reason as to why a complex II inhibitor such as LND and the comparative TTFA differ so very much in terms of their response when bound. TTFA when bound elicits an inhibitory growth curve (Figure 9A). On the other hand, LND when bound mimics the WT until stationary phase when it causes severe aggregation (Figure 7A). Lysine Succinylation could be the signalling mechanism that allows LND to cause global effects within the cell.

4.1 Inhibition of SDH affects growth and viability of *C. glabrata*

Two drugs (TTFA and LND) that are reported to target SDH activity were used and tested to see how active the SDH enzyme itself is when treated with complex II inhibitors. By measuring how active the SDH enzyme is, this gives reassurance that firstly the drug is having an effect on the enzyme and secondly how much of an effect LND can produce on the enzyme when bound. The reduction of a tetrazolium salt such as Blue Tetrazolium Chloride (BT) is the most suitable way by providing substrate for the SDH enzyme and the measurement being how much of the tetrazolium salt is being reduced to formazan. Both TTFA and LND showed a huge reduction in tetrazolium conversion to formazan compared to the wild type. More surprising is that LND showed to be a greater inhibitor for this assay to that of the TTFA. This confirmed that both drugs are having an inhibitory effect on the SDH enzyme,

but it could be said purely from this one experiment if this temporarily inactive SDH enzyme would cause cells to remain viable or not. It is a common mistake to take the absorbance values from a colorimetric assay such as this and perform a cell viability calculation ((Absorbance$_{sample}$ – Absorbance$_{blank}$)/ (Absorbance$_{control}$ – Absorbance$_{blank}$)x100) and assume this is the true viability percentage of each sample. The issue with this is that it does not consider whether the cells may be stuck in a mutational cell cycle whereby the cells can perfectly form formazan by conversion of tetrazolium, but it would not be able to form colonies, thus it is not truly viable. It is not uncommon for cells such as *Candida* to be very plastic when inhibitors are introduced to them and this is something that needs to be taken into consideration with this assay.

Coupling the BT assay with the viability assay allows the project to confidently state that firstly the drug is having an effect on the SDH enzyme and secondly whether the complex II inhibitor is having an effect on viable cells to form colonies. If the BT assay was a true representation of viable cells, then it would be expected to mirror the results shown in both assays, but this is not the case. The BT assay (Figure 10) showed nearly fully diminished SDH activity for both LND and TTFA treated cells but this reduction is not seen in the viability assay (Figure 11). This suggests that whilst the cells are temporarily disrupted as the drugs are bound to complex II, the cells are able to recover from this disruption but not completely. The question that arose from the coupled experiment is what mechanisms were occurring to allow for the cells to partially overcome this mitochondrial dysfunction. It has already been shown that during the cellular aging process, *S. cerevisiae* shows an increased SDH activation by more than

50% as well as glyoxylate related enzyme activation such as ICL1 and MLS. This selection allows cells to reveal the mechanism of their higher viability as caused by shunting of complete Krebs cycle by glyoxylate cycle, with a concomitant increased rate of the most efficient energy source, namely succinate formation and oxidation (Samokhvalov, Ignatov and Kondrashova, 2004).

The *C. glabrata* clinical isolates showed a lot of variation in their growth curves. Isolates *CG30261* and *CG027884* produced a curve which suggests inhibitory effects with LND but *CG2509* and *CG028987* produced a growth curve which that mimicked the *WT*. This highlights the unpredictable results which can come from using clinical isolate studies (in-vivo) compared to laboratory strains (in-vitro). As this project uses four clinical isolates which have already shown varying genotypic characteristics in the growth assays, there could be potential for a significant degree of plasticity, depending upon the genotype and different environmental pressures. The solvent control showed that DMSO led to a pronounced inhibition of growth in all four clinical isolates, this was also observed in the LND treatment and so growth reduction may be due to DMSO alone. Statistical analysis was not performed so it cannot be said whether this happened purely by. It would have also been ideal to repeat the same experiment at varying temperatures in order to see if there was any difference in growth and not just at 37^{o}C (replicating the temperature of the average human body).

For all four isolates, the trace of the curve as shown by the increased peaks and troughs becoming wider could suggest aggregation and this is not seen in the solvent control, so it suggests it is solely from LND. The growth curves were not statistically analysed and the data for each clinical isolates technical repeats are no longer available so it cannot be said that this did not occur purely by chance. The result does show that the trace in question was apparent in all four of the different clinical isolates treated with LND so a future suggestion would be to produce technical repeats of all four clinical isolates to highlight if this could be due to noise associated with the equipment and the protocol. Aggregation was seen visibly in the cells when they appeared to be growing in clump formation and the visible clumping shown consistently in the wells when taking out of the plate reader during experiments. This is important as the cell wall appears to have been affected if this is to be true, causing cell walls of neighbouring cells to stick together and adhesin molecule activity being potentially enabled. As mitochondrial function is linked to the aggregation phenotypes (Dhar, R. 2020), possibly mitochondrial damage has caused enabling of cell wall integrity pathway. As the mitochondria is also involved in lipid maturation, these damaged cells may have reduced lipid synthesis that is usually sent to the cell's membrane. The cells maybe sensing this change and responding by an internal stress response which in turn would repair the plasma membrane and cause a shift into defensive mode via clumping.

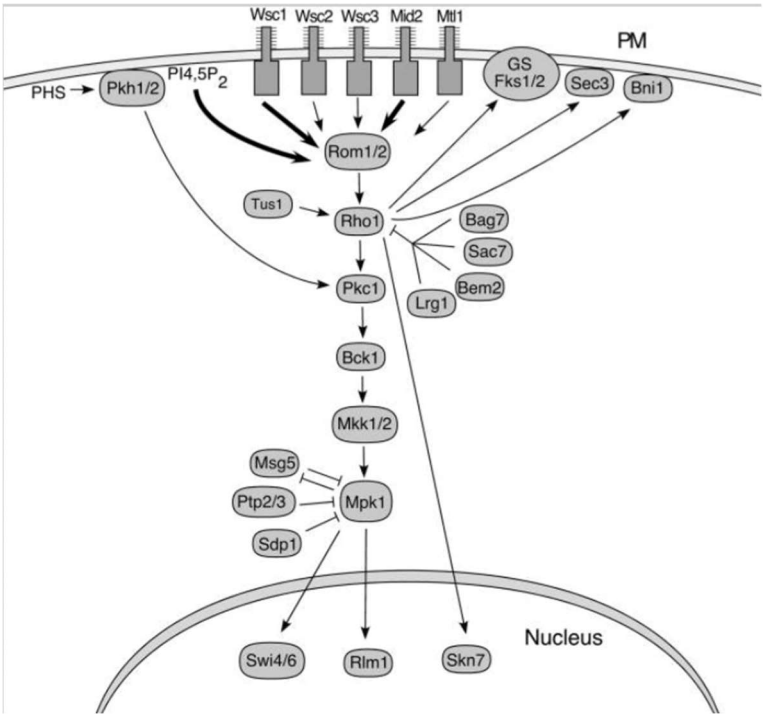

Figure 23. An overview of the cell wall integrity pathway (Philip and Levin, 2001).

The mechanisms behind the cell wall integrity pathway (CWI) (Figure 23) are well documented and drugs are already known to have effects along the cascade. Caffeine has shown to induce phosphorylation of Mpk1p and was accompanied by a negligible activation of its main downstream target, the Rlm1p transcription factor. This result was consolidated by the finding that the loss of RLM1 had no consequence on the increased resistance of caffeine-treated cells to zymolyase, indicating that the cell wall modification caused by this drug is largely independent of transcriptional activation of Rlm1 upregulated genes (Kuranda *et al.*, 2006).

There is literature that links the state of the mitochondria and the changes of the cell wall (Xia, M. F. *et al*. 2019) and this could might explain why this flocculation occurs. Notably, it has been reported that high osmolarity glycerol pathway

(Hog1p) activation mediates mitochondrial dysfunction and catalase A deficiency associated with oxidative stress sensitivity and premature aging of inositol phosphosphingolipid phospholipase C (isc1) cells. Downstream of Hog1p, Isc1p deficiency activates the CWI pathway. Deletion of the SLT2 gene, which encodes for the MAPK of the CWI pathway, was lethal in *⊿isc1* cells and this mutant strain was hypersensitive to cell wall stress. However, the phenotypes of *⊿isc1* cells were not associated with cell wall defects. This supports a role for Hog1p in the regulation of mitochondrial function and suggest that constitutive activation of Hog1p is deleterious for *⊿isc1* cells under oxidative stress conditions and during chronological aging (Barbosa et al., 2012).

It has also been shown that signalling from the mitochondria to affect the cell wall involves ANAC017, a transcription factor important in retrograde signalling to the nucleus upon mitochondrial dysfunction (Hu *et al.*, 2016). This work provided some insight into a mechanism which could explain both how the cells are able to respond to mitochondrial dysfunction but also link the aggregation to mitochondrial disruption.

A further experiment that could have been performed to test if there was a link between the TCA cycle function and cell wall structure would be to grow TCA single deletion mutants to represent a strain with each of the main TCA enzymes missing as seen in figure 19A. Once the cells were subcultured to OD_{600} 0.1 and the subculture grown to stationary phase, they could be stained with Congo red (CR) and Calcofluor white (CFW). The rationale is that the cell wall mutants are sensitive to these two related anionic dyes. They interfere with

the construction and stress response of the cell wall and would allow for microscopy analysis to view how each strains cell wall looks compared to a wild type. By comparing the strains, it would have given a good insight into which strain could potentially have the most dependence on when the cell responds to stresses.

Rapamycin has also shown to have effects on the TOR (target of rapamycin) pathway. TOR controls cell growth in response to nutrient availability and inactivation of TOR function by rapamycin or nutrient exhaustion is accompanied by triggering various cellular mechanisms aimed at overcoming the nutrient stress (Torres *et al.*, 2002). In *S. cerevisiae*, the protein kinase C (PKC)-mediated mitogen-activated protein kinase pathway is regulated by TOR function because upon specific Tor1 and Tor2 inhibition by rapamycin, Mpk1 is activated rapidly in a process mediated by Sit4 and Tap42. Osmotic stabilization of the plasma membrane prevents both Mpk1 activation by rapamycin and the growth defect that occurs upon the simultaneous absence of Tor1 and Mpk1 function, suggesting that TOR inhibition is sensed by the PKC pathway at the cell envelope. This process involves activation of cell surface sensors, Rom2, and downstream elements of the mitogen-activated protein kinase cascade. Rapamycin also induces depolarization of the actin cytoskeleton through the TOR proteins, Sit4 and Tap42, in an osmotically suppressible manner. During entry into stationary phase, a physiological situation of nutrient depletion, also leads to the activation of the PKC pathway, and Mpk1 has shown to be essential for viability once cells enter G0 (Torres et al., 2002). As shown by Rapamycin, during stationary phase for when nutrients are depleted and resulting in the

activation of the PKC pathway, Mpk1 seems to be the main drug target and this could be where the severe aggregation that LND causes could be potentially inducing. In order to have tested this theory, it would have been useful to perform a western blot to analyse whether LND treated cells had varying difference of band intensity than that of untreated cells. Having seen flocculation accumulation, a Western blot analysis would state whether LND alone had affected the cell wall by inducing the CWI signalling at the point of the MpK1 enzyme.

TTFA produced a much cleaner growth curve and shows a very clear inhibitory growth curve compared to WT. Solvent control showed that ethanol alone did not produce this growth inhibition. TTFA showed very potent inhibitory effects (Figure 9A) compared to wild type. This confirmed that complex II when disrupted can have significant anti-fungal properties but also that complex II inhibitors have very different effects within the cell. Flocculation as seen with LND treated cells was not seen with TTFA treated cells or with either DMSO or ethanol treated cells, so this confirmed that the flocculation is specific to LND. The growth curve which was performed using *S. cerevisiae* and LND failed due to equipment malfunctioning, so it was not possible to show whether this flocculation was species specific. For future work, it would be interesting to simply perform a growth curve assay using LND with *S. cerevisiae* in order to answer this.

Another growth assay for future work would be to combine LND with N-acetyl-cysteine (NAC) which is known to salvage ROS and see the time difference between cell death of NAC treated and NAC untreated with LND.

4.2 Inhibition of SDH affects *C. glabrata* biofilm formation

C. glabrata biofilms are important as they are the species main form of virulence as an opportunist pathogen. The biofilm is utilised as a means of defence against both drugs and allow for the compact layer of cells to colonise on medical equipment such as tracheostomy tubes or on wounds that a patient may have. By reducing the biofilm formation or disrupting a mature biofilm, it could hinder the pathogen or at least reduce the opportunity for it to invade an immunocompromised patient.

Following the flocculation finding, it was worth investigating if the growth defects that occurs from potential cell wall stress could be having a knock-on effect on the cells ability to cooperate with neighbouring cells to form a mature biofilm. Whether overly induced adhesin molecule synthesis could lead to an increase in a biofilm's structural integrity or whether LND's apparent cellular disruptions could be more inhibitory on a biofilm's population than its very minimal inhibitory effects on a *C. glabrata* single cell. Upon staining of crystal violet after 2 days of treatment with both complex II inhibitors, both partially reduced the ability of *C.*

glabrata to form a mature biofilm. TTFA has already shown to be a very useful in reduction of biofilms in other species such as *B.subtilis* (Qin *et al.*, 2019).

As *C. glabrata* utilises the biofilm as its most virulent factor, biofilm reduction is a vital anti-fungal property which makes LND a very appealing drug for future research as many investors in the healthcare setting such as Doctors and Dentists have to overcome biofilm formation regularly among their patients. For future work, it would be ideal to repeat the experiment but add LND after 24 hours of incubation to see how the drug can effect a biofilm which has already begun to mature, as previously stated that the *C. glabrata* biofilm is rich in a mesh of both carbohydrates and proteins, this could hinder LNDs ability to reach the cells to have its desired effects. This project can only state that LND disrupts biofilm formation if administered in the early stages of formation.

4.3 Inhibition of SDH by LND does not lead to respiratory disruption in *C. glabrata*

The spike after LND is administered during the respirometry analysis (Figure 13B) represents a transient increase in flow of electrons through the chain. This led to investigating whether the SDH inhibition may be causing a reliance upon the NADH Dehydrogenase Internal (NDI1) (complex I equivalent in *C. glabrata*). This was ruled out after a combination of Flavone and LND produced transient uncoupling but no permanent disruption in respiration was observed.

The finding that SDH inhibition does not lead to respiratory disruption was quite an interesting and unexpected finding considering how effective it has been shown in the BT assay to inhibit the SDH enzyme activity (Figure 10) and how reliant both LND and TTFA have shown in literature to produce ROS in DB-1 melanoma cell line cells (Guo *et al.*, 2016). This could suggest that yeast suggests yeast cells have evolved to monitor metabolism at these points in the mitochondria, to try and re-wire metabolism to remain viable and when disrupted. As in the case of LND, markers of poor cellular health e.g., growth defects such as slower doubling times which suggests metabolic re-wiring (Figure 8), the production of ROS (as seen in *S. cerevisiae WT* and mutants in Figure 19A) and loss of viability (Figure 11) have occurred. These all suggest that finding the compensatory points of metabolism to target for future drug development may be the way to progress.

4.4 Inhibition of SDH does not lead to ROS accumulation in *C. glabrata*

The most surprising finding of the *C. glabrata* experiments was that LND treated cells produced regular levels of ROS compared to wild type and especially nowhere near the levels which could be deemed lethal or induce cellular stress. This contradicted literature that showed that measuring of ROS formation by reduced FAD or ubiquinone site by use of a DCF fluorescence produced ROS levels higher in LND than that of TTFA treated cells. (Guo *et al.*, 2016). The result is surprising as it was expected that LND would induce ROS within the

complex II by means of ubiquinone reduction, similar to TTFA but to produce a higher level of ROS production than TTFA when TTFA has shown to be a more potent inhibitor for complex II. This finding suggests that *C. glabrata* do not utilise the ETC when SDH is inhibited and supports the theory in section 4.3 which suggests that a disruption along the ETC causes re-wiring of the metabolic pathway.

For future work it would be crucial to repeat the same experiment to see if the same result occurs and also to run the same experiment but to use NPA (a succinate analogue which inhibits succinate-oxidation enzymatic activity) and TTFA (inhibition occurs by binding of TTFA to two ubiquinone binding sites) on *C. glabrata*. This would rule out whether this is a conserved response to LND or whether it is a general response to complex II inhibitors with differing mechanisms of actions.

4.5 SDH2 and IDH2 produce the highest number of ROS cells amongst the *S. cerevisiae* TCA cycle

The flow cytometry analysis of the *S. cerevisiae* TCA single knockout mutants showed that IDH2 and SDH2 enzymes are important intermediates of the TCA cycle and without their presence cause the highest ROS cells. This gave assurance that the SDH does in fact play a crucial role in the cells energy homeostasis and would be the ideal drug target compared to IDH due to the severe illnesses linked to IDH dysfunction. Mutation of IDH1 and IDH2 have

already been identified through exome sequencing of colon tumor and glioblastoma multiforme (GBM) (Parsons *et al.*, 2008). Since these discoveries, IDH mutations have been observed in several other tumor types, including acute myeloid leukemia (AML), chondrosarcoma, and intrahepatic cholangiocarcinoma. Currently, phase I studies of mutant IDH inhibitors are currently ongoing in patients with IDH-mutant hematologic and solid tumors, with early data in hematologic tumors suggesting a manageable safety profile as well as clinical benefit. Inhibition of mutant IDH shows promise as a treatment approach in hematologic malignancies, with further development ongoing in solid tumors and glioma. The mutant IDH inhibitors may have clinical utility both as single agents and in combination strategies that target additional oncogenic pathways (Dang, Yen and Attar, 2016). The flow cytometry data was not statistically analysed due to time constraints so it cannot be said whether it happened by chance. For future work, it would be beneficial to create *C. glabrata* transformants with single knockout mutants of the TCA cycle in order to see whether both species share the same ROS characteristics. The TTFA treated cells (Figure 18) led to a very pronounced effect in stationary phase that may suggest a complete loss of respiration in *S. cerevesiae*, so this future work could confirm if *S. cerevisiae* and *C. glabrata* respond differently to LND.

4.6 Retrograde pathway (RTG) enabling upon administration of LND

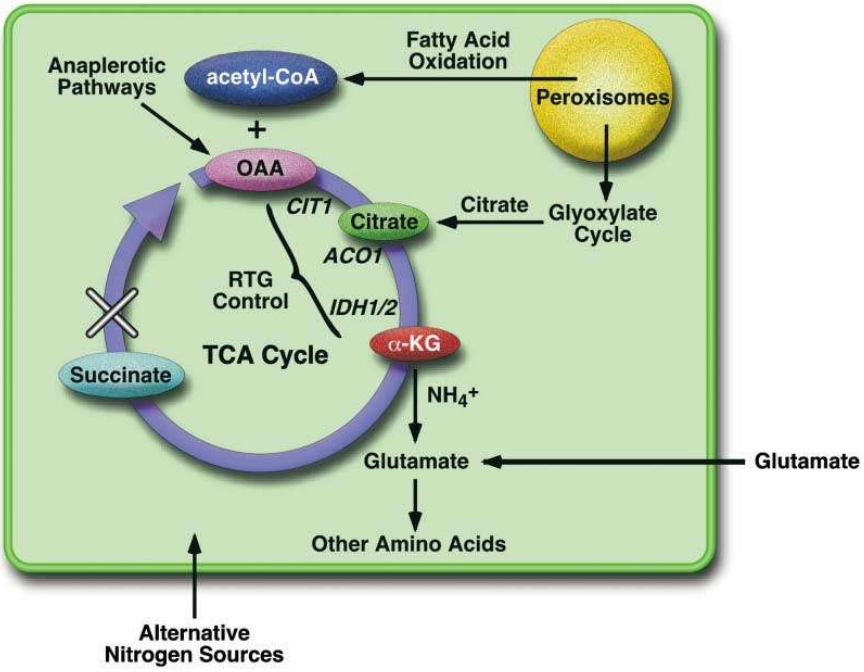

Figure 24. The retrograde pathway enables respiratory- deficient cells to maintain glutamate supplies by providing substrates for α-ketoglutarate.

As the project has been shown that there is some effect on growth and viability upon SDH inhibition, it led to investigating the role of compensatory pathways. The RTG and glyoxylate cycle could potentially be the systems in which future work could design a rational inhibitory drug combination. The first step was to carry out the following study.

The most detailed information on the mechanism of retrograde signalling comes from studies of the *CIT2* gene. Since its discovery as a retrograde-responsive gene (Liao et al., 1991), *CIT2* has served as a prototypical readout for the yeast retrograde response. The ONPG assay allows for allows colorimetric measuring of the activity of the *CIT2* promoter which is an indicator for β-galactosidase activity (retrograde signalling), all the single knockout *cit2-lacz* transformants

were examined to see whether LND was causing an upregulation of the RTG in response to a faulty TCA cycle. Upon administration of LND, all mutants saw an increase in CIT2 levels except for *⊿icl1* (which is located within the glyoxylate cycle). This suggests that ICL1 mediates the glyoxylate cycle and ultimately without it, the cells would not be able to synthesis the necessary intermediates by utilising other carbon sources.

A study has already shown the effects of *icl1* deletion on *C. glabrata* and it seems to show similar effects as shown by the *S. cerevisiae* analysis in this project. The study showed that that disruption of *icl1* rendered *C. glabrata* unable to utilise acetate, ethanol or oleic acid. In addition, *∆icl1l* cells displayed significantly reduced biofilm growth in the presence of several alternative carbon sources. It was also found that *icl1* is crucial for the survival of *C. glabrata* in response to macrophage engulfment. Disruption of *icl1* also conferred a severe attenuation in the virulence of *C. glabrata* in the mouse model of invasive candidiasis (Chew *et al.*, 2019). The study concluded that a functional glyoxylate cycle is essential to utilise certain alternative carbon sources in vitro and to display full virulence in vivo. Also, as macrophage engulfed *C. glabrata* have shown that key metabolic enzymes in the glyoxylate cycle were ICL1 and MLS1. (Chew, Chee and Than, 2019), by inhibiting ICL1, it would suggest that it would render the pathogen more vulnerable to the immune response within humans. To see the importance of ICL1 in both species reinforces the rationale that ICL1 inhibitors could be a potential anti-fungal drug for the future, whether in combinational drug therapy with a drug such as LND or not would have to be tested.

4.7 Mitochondrial Succinyl-CoA may cause global cellular effects via Succinylation

One finding which still needs answering from this is project is what mechanism of action LND has due to its effects not being related to respiration. Unlike TTFA which seems to produce high ROS via the ETC. One theory is how Succinylation could be the modification that is causing global cellular effects and is mediated within the mitochondria. This would suggest that Succinyl-CoA would in fact be more important than Succinate with regards to LND's future as a potential anti-fungal treatment.

Succinylation is a posttranslational modification where a succinyl group (-CO-CH2-CH2-CO2H) is added to a lysine residue of a protein molecule. Succinylation is an area with very little research but could be just as much important for cellular signalling as acetylation. Lysine Succinylation has been previously shown to occur in the active site of homoserine trans-succinylase (Rosen *et al.*, 2004). What still remains a mystery are both the mechanisms of action of Succinylation and the Succinyl donor to Lysine.

More recently a very in-depth analysis of Succinylation sites in *S. cerevisiae,* uncovered that what was previously understood in terms of the number of Succinylation sites was in fact far lower than there actually is. Previous studies suggested that there were 4 proteins and 7 Succinylation sites (Xie *et al.*, 2012) but recently it has shown that there is in fact 474 proteins and 1345 Succinylation sites in *S. cerevisiae* (Weinert *et al.*, 2013). Considering that is

also shown that any slight changes in Succinyl-CoA within the mitochondria causes changes in every Lysine Succinylation site globally (Weinert *et al.*, 2013) and also considering that any abundant protein with a Lysine residue is able to perform Lysine Succinylation, this highlights just how impactful LND acting on SDH to increase Succinyl-CoA levels within the mitochondria can be.

As Succinyl-CoA and succinate are mainly formed in the mitochondria via the TCA cycle or by fatty acid oxidation, this would suggest that defects within the TCA cycle that result in differing levels of Succinyl-CoA would produce global effects which are indirectly related to the mitochondria. If this was occurring, it would suggest that changes would be impacted are within the cytoplasm, nuclear expression or cell wall rearrangements. The key enzymes of the TCA cycle which have most effect on Succinyl-CoA levels are the enzymes KGD1, LSC1 and SDH2 (Figure 24).

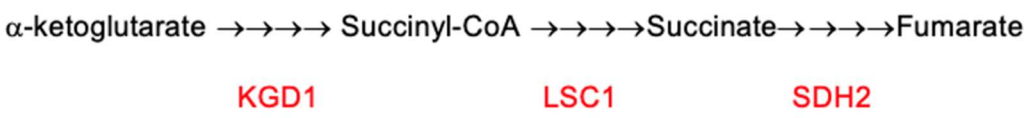

Figure 24. A view of the important steps (as seen in black) and the enzymes (as seen in red) involved with Succinyl-CoA within the TCA cycle.

α-ketoglutarates conversion to succinyl-CoA occurs by the α-ketoglutarate dehydrogenase complex (composed of KGD1, KGD2, and LPD1). Succinyl-CoA is then converted to Succinate by succinyl-CoA ligase (LSC1 is the α subunit and LSC2 is the β subunit of the complex). Succinate undergoes catalysed oxidation of fumarate in the TCA which in turns donates electrons to ubiquinone in the inner mitochondrial membrane. A theory which is yet to be tested in this

project due to time restraints is that inhibiting complex II plays a major role in the glyoxylate RTG signalling via Succinylation. The *⊿kgd1* strain lowers Succinyl-CoA levels as the essential enzyme to convert it is missing which means KGD levels pool within the TCA cycle, the opposite effects occur with *⊿lsc1* as Succinyl-CoA can not be converted to Succinate so pooling of Succinyl-CoA occurs. This is already apparent as it has been shown that *⊿kgd1* mutant grown on galactose media shows a 4-fold decrease in global Lysine Succinylation and a 6-fold mitochondrial Lysine Succinylation (Weinert *et al.*, 2013). In contrast, *⊿lsc1* mutant showed a 3-fold increase in global Lysine Succinylation and a 3-fold increase Lysine Succinylation (Weinert *et al.*, 2013). Furthermore, one step further in the TCA cycle is overlooked as SDH inhibition would also inhibit the reversible conversion of Succinate to Succinyl-CoA levels. Any deficiency within these enzymes greatly impact Succinyl-CoA. Another question for further experiments would be if Succinyl-CoA acts as a regulator and can traverse the Mitochondrial membrane when levels are high or if levels are low within the mitochondria then cytoplasmic Succinyl-CoA can be salvaged in. If this were the case, this could suggest that depleted Succinyl-CoA by SDH2 inhibitors such as LND are quickly replenished if the drug is not as potent as TTFA.

Another question is if *S. cerevisiae* infact do not have any form of succinyl-transferase then this suggests that Lysine Succinylation occurs to chemical modification and would suggest that is it permanent and unreversible.

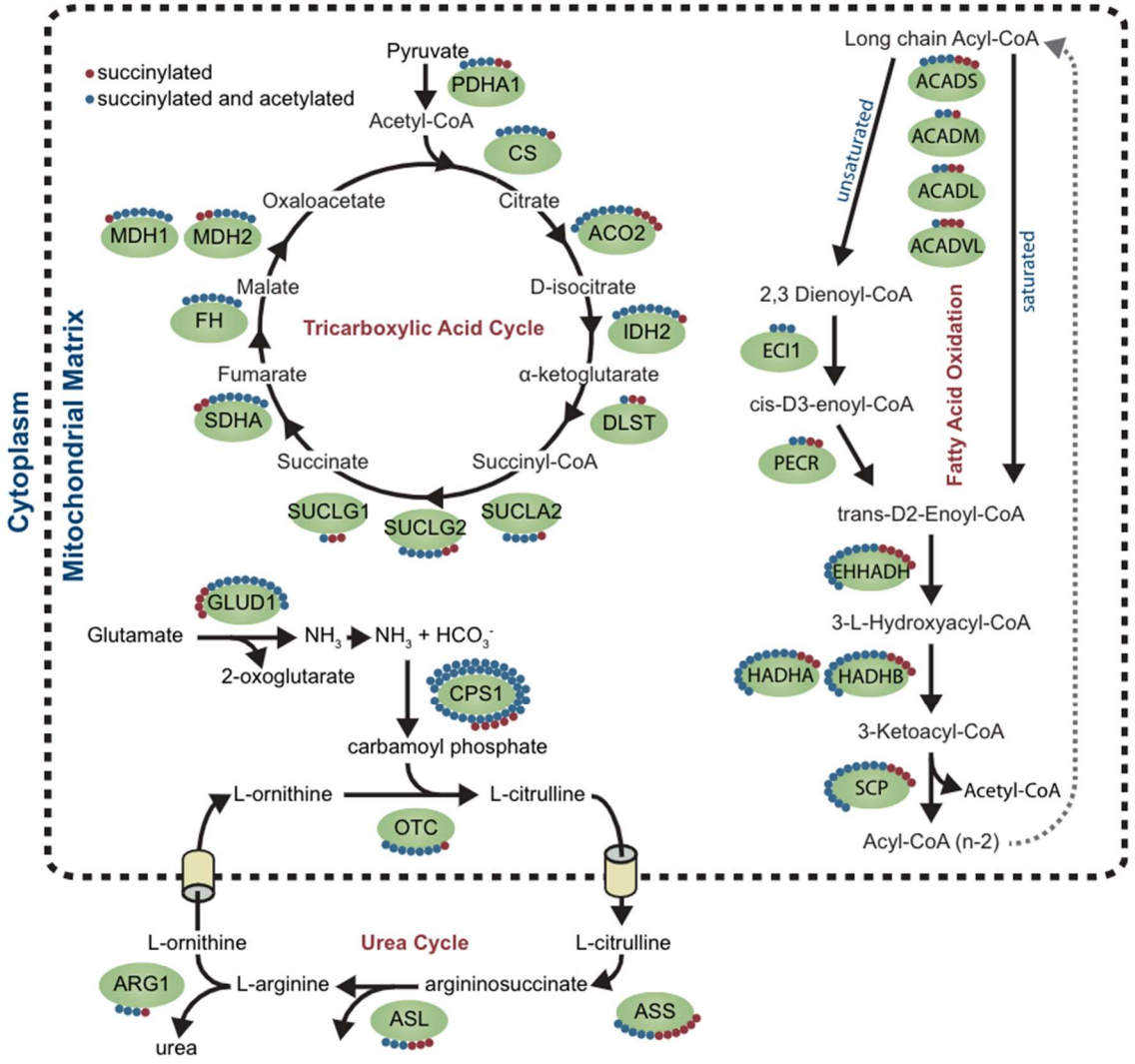

Figure 25. Succinylation of Enzymes involved in the Tricarboxylic Acid Cycle, the Urea Cycle, and Fatty Acid Oxidation. Succinylated enzymes identified in mouse liver tissue are shown in green ovals, sites that were found to be both acetylated and Succinylated are shown as blue circles, sites only found to be Succinylated are shown as red circles. The enzymes shown are pyruvate dehydrogenase component subunit alpha (PDHA1), citrate synthase (CS), aconitate hydratase (ACO2),isocitrate dehydrogenase (IDH2), dihydro-lipoamide S-succinyl transferase (DLST), succinyl-CoA ligases G1, G2, and A1 (SUCLG1, SUCLG2,and SUCLA1), succinate dehydrogenase (SDHA), fumarate hydratase (FH), malate dehydrogenase 1and 2 (MDH1 and MDH2), glutamate dehydrogenase (GLUD1), carbamoyl phosphate synthetase I(CPS1), ornithine transcarbamoylase (OTC), argi-ninosuccinate synthetase (ASS), argininosucci-nate lyase (ASL), arginase 1 (ARG1), short-,medium-, long-, and very-long-chain-specificacyl-CoA dehydrogenases (ACADS, ACADM,ACADL, and ACADVL), enoyl-CoA delta isom-erase 1 (ECI1), peroxisomaltrans-2-enoyl-CoAreductase (PECR), enoyl-CoA hydratase/3,2-trans-enoyl-CoA isomerase,3-hydroxyacyl-CoAdehydrogenase (EHHADH), long-chain enoyl-CoAhydratase, long-chain 3-hydroxyacyl-CoA dehy-drogenase alpha and beta

(HADHA and HADHB),and nonspecific lipid-transfer protein (SCP) (Weinert *et al*., 2013)

The interesting point to take from the ONPG data (Figure 22) and the mouse liver data shown (Figure 25) is that the promising enzymes found in ONPG correspond with those with the majority Succinylation sites to Acetylation sites in both the TCA cycle and the fatty acid oxidation. This further suggests that *CIT2* levels via the glyoxylate cycle could in fact caused by Succinylation. The defected TCA cycle caused Succinyl-CoA levels to be the key factor. Steps before Succinyl-CoA in the TCA cycle generally show a lowered level of CIT2 compared to those enzymes after Succinyl-CoA and especially those enzymes found within the glyoxylate cycle.

4.8 Investigating *LSC2* for conserved fungal specific regions

From the Succinylation investigation that highlighted that LSC as an enzyme caused an upregulation of Succinylation by means of Succinyl-CoA and also from the *⊿lsc2* growth curve (Figure 18D) which showed the most shallow log phase of all mutants and also the loss of respiration in stationary phase, this led to investigating further if the DNA sequence of LSC2 had any conserved fungal specific regions which could be targeted in future combinational drug therapy with LND.

Figure 26. Highlighting the fungal specific Tyrosine in LSC2 which was conserved within fungal species and not present in both *H. sapiens* and *H. musculus.*

The tyrosine is quite an interesting amino acid to be conserved as it's a phosphorylation residue. It could be a relatively simple residue to modify and this led to investigating the structure of the *S. cerevisiae* LSC2 in comparison to the *H. sapiens* equivalent. The fungal specific tyrosine in Figure 27 can be seen highlighted in red.

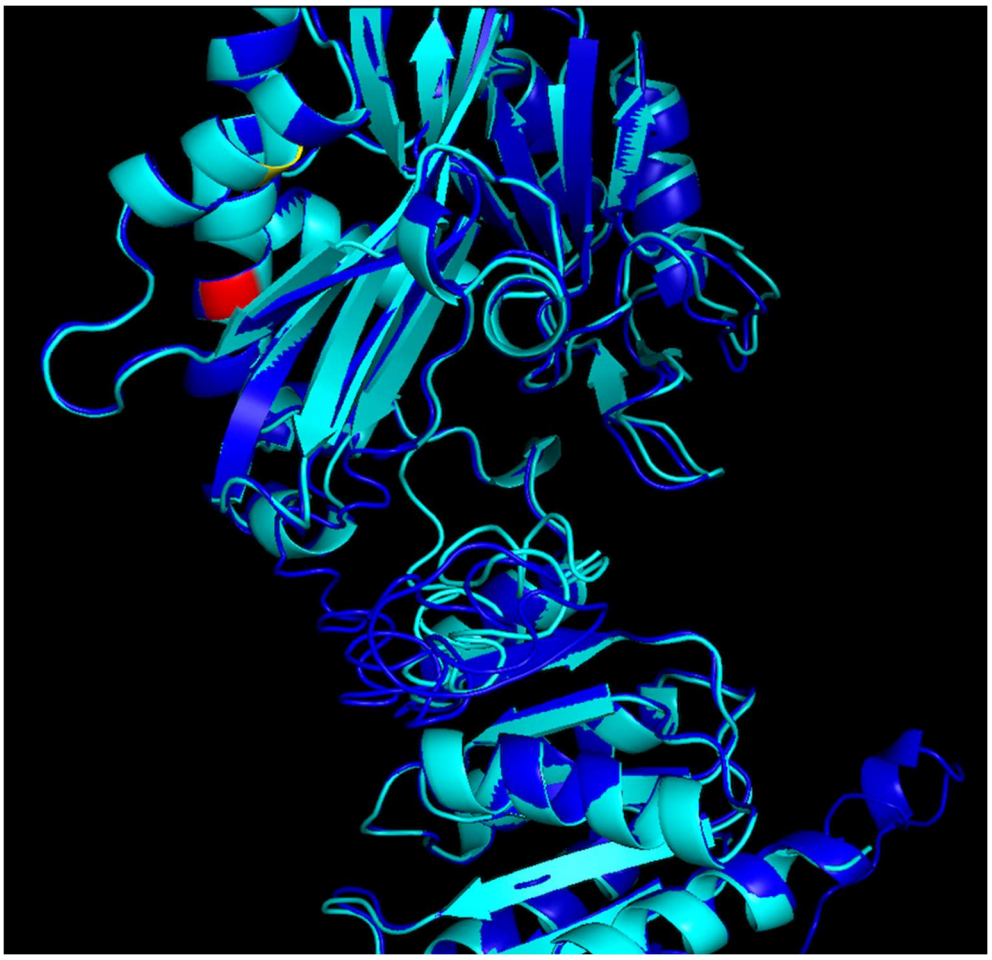

Figure 27. A PyMOL overlay structures of the beta subunits of Succinate ligase in *H.sapiens* and *S.cerevisiae*. The fungal specific Tyr seen in red.

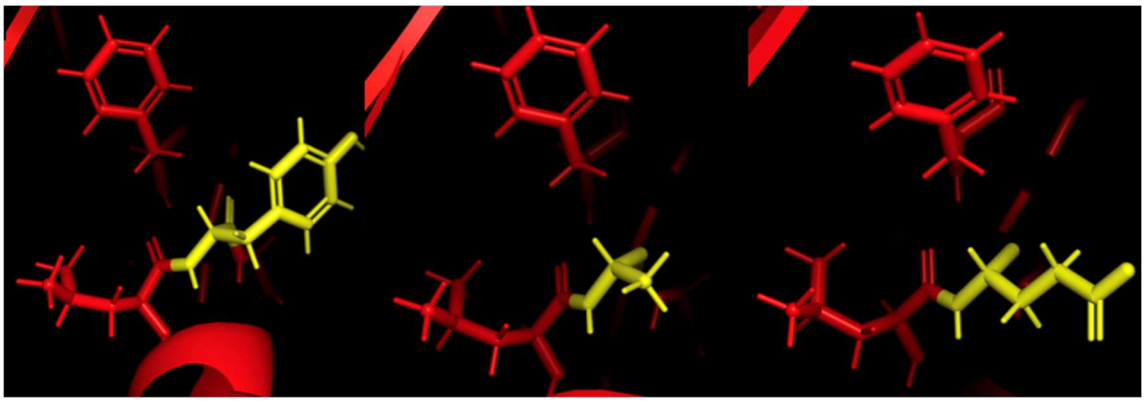

Figure 28. (A) A PyMOL stick view of the fungal specific Tyrosine. (B) Tyrosine replaced with an Alanine. (C) Tyrosine replaced with a Glutamate.

Residue modifications were performed to replace the fungal specific Tyrosine with either an Alanine or Glutamate. Due to time constraints, this investigation could not be continued. For future work, it would be beneficial to mutate the residue to alanine (which cannot be phosphorylated) or glutamate (which acts as a mimic of the phosphate group presence) and see what the effects are within LSC2. Protein phosphorylation is an important cellular regulatory mechanism as many enzymes and receptors are activated/deactivated by phosphorylation and dephosphorylation events, by means of kinases and phosphatases. Such inhibitors as the kinase inhibitors have been shown to be valuable for the treatment of cancer (Ardito et al., 2017). It would be ideal to see if it would be as beneficial in the fungal model. If the mutation of this residue led to a loss in SDH activity or loss of fitness, then would be worth approaching as a target. Future research would be crucial to find out what the residue does. Questions which would need answering are if it effects SDH assembly or interaction with substrate? Or whether it has any impact on stability or degradation?

4.9 Concluding remarks

LND has shown to cause significant anti-fungal properties which warrant future investigations. Such as its pronounced reduction in the *C. glabrata* biofilm and its ability to reduce colony formation whilst causing flocculation which indicate cell wall stress responses. Despite LND showing through respirometry analysis that *C. glabrata* not utilise the ETC when SDH is inhibited, it does suggest that it force a reliance on the glyoxylate cycle. Through *S. cerevisiae* mutant studies,

weak points within the glyoxylate the project were found to be ICL1 (within the glyoxylate cycle) and LSC2 (within the TCA cycle). Future research on combinational drug therapy of using LND alongside inhibitors of ICL1 or LSC2 would be crucial.

References

1. Alexander, B. D. *et al.* (2013) 'Increasing echinocandin resistance in candida glabrata: Clinical failure correlates with presence of FKS mutations and elevated minimum inhibitory concentrations', *Clinical Infectious Diseases*. doi: 10.1093/cid/cit136.
2. Ardito, F. *et al.* (2017) 'The crucial role of protein phosphorylation in cell signalingand its use as targeted therapy (Review)', *International Journal of Molecular Medicine*. doi: 10.3892/ijmm.2017.3036.
3. Barbosa, A. D. *et al.* (2012) 'Activation of the Hog1p kinase in Isc1p-deficient yeast cells is associated with mitochondrial dysfunction, oxidative stress sensitivity and premature aging', *Mechanisms of Ageing and Development*. doi: 10.1016/j.mad.2012.03.007.
4. Barros, M. H., Netto, L. E. S. and Kowaltowski, A. J. (2003) 'H 2 O 2 generation in Saccharomyces cerevisiae respiratory pet mutants: Effect of cytochrome c', *Free Radical Biology and Medicine*. doi: 10.1016/S0891-5849(03)00307-1.
5. Bhattacharya, K. *et al.* (2014) 'Mahanine, a novel mitochondrial complex-III inhibitor induces G0/G1 arrest through redox alteration-mediated DNA damage response and regresses glioblastoma multiforme', *American Journal of Cancer Research*.
6. Brun, S. *et al.* (2004) 'Mechanisms of Azole Resistance in Petite Mutants of Candida glabrata', *Antimicrobial Agents and Chemotherapy*. doi: 10.1128/AAC.48.5.1788-1796.2004.
7. Brun, S. *et al.* (2005) 'Biological consequences of petite mutations in Candida glabrata', *Journal of Antimicrobial Chemotherapy*. doi: 10.1093/jac/dki200.
8. Butler, G. *et al.* (2009) 'Evolution of pathogenicity and sexual reproduction in eight Candida genomes', *Nature*. doi: 10.1038/nature08064.
9. Castanheira, M. *et al.* (2017) 'Monitoring antifungal resistance in a global collection of invasive yeasts and molds: Application of CLSI epidemiological cutoff values and whole-genome sequencing analysis for detection of azole resistance in Candida albicans', *Antimicrobial Agents and Chemotherapy*. doi: 10.1128/AAC.00906-17.
10. Cheng, G. *et al.* (2019) 'Targeting lonidamine to mitochondria mitigates lung tumorigenesis and brain metastasis', *Nature Communications*. doi: 10.1038/s41467-019-10042-1.
11. Chew, S. Y. *et al.* (2019) 'Glyoxylate cycle gene ICL1 is essential for the metabolic flexibility and virulence of Candida glabrata', *Scientific Reports*. doi: 10.1038/s41598-019-39117-1.
12. Chew, S. Y., Chee, W. J. Y. and Than, L. T. L. (2019) 'The glyoxylate cycle and alternative carbon metabolism as metabolic adaptation strategies of Candida glabrata: Perspectives from Candida albicans and Saccharomyces cerevisiae', *Journal of Biomedical Science*. doi: 10.1186/s12929-019-0546-5.
13. Cleveland, A. A. *et al.* (2012) 'Changes in incidence and antifungal drug resistance in candidemia: Results from population-based laboratory

surveillance in Atlanta and Baltimore, 2008-2011', *Clinical Infectious Diseases*. doi: 10.1093/cid/cis697.
14. Dang, L., Yen, K. and Attar, E. C. (2016) 'IDH mutations in cancer and progress toward development of targeted therapeutics', *Annals of Oncology*. doi: 10.1093/annonc/mdw013.
15. De Groot, P. W. J. *et al.* (2008) 'The cell wall of the human pathogen Candida glabrata: Differential incorporation of novel adhesin-like wall proteins', *Eukaryotic Cell*. doi: 10.1128/EC.00284-08.
16. Dhar, R. (2020) 'Role of Mitochondria in Generation of Phenotypic Heterogeneity in Yeast', *Journal of the Indian Institute of Science*. doi: 10.1007/s41745-020-00176-3.
17. Ferrari, S. *et al.* (2009) 'Gain of function mutations in CgPDR1 of Candida glabrata not only mediate antifungal resistance but also enhance virulence', *PLoS Pathogens*. doi: 10.1371/journal.ppat.1000268.
18. Ferrari, S. *et al.* (2011) 'Loss of mitochondrial functions associated with azole resistance in Candida glabrata results in enhanced virulence in mice', *Antimicrobial Agents and Chemotherapy*. doi: 10.1128/AAC.01271-10.
19. Fidel, P. L., Vazquez, J. A. and Sobel, J. D. (1999) 'Candida glabrata: Review of epidemiology, pathogenesis, and clinical disease with comparison to C. albicans', *Clinical Microbiology Reviews*. doi: 10.1128/cmr.12.1.80.
20. FLORIDI, A. *et al.* (1988) 'Lonidamine-Induced Membrane Permeability and the Effect of Adriamycin on the Energy Metabolism of Ehrlich Ascites Tumor Cells', *Annals of the New York Academy of Sciences*. doi: 10.1111/j.1749-6632.1988.tb22350.x.
21. Grant, C. M., MacIver, F. H. and Dawes, I. W. (1997) 'Mitochondrial function is required for resistance to oxidative stress in the yeast Saccharomyces cerevisiae', *FEBS Letters*. doi: 10.1016/S0014-5793(97)00592-9.
22. Guo, L. *et al.* (2016) 'Inhibition of mitochondrial complex II by the anticancer agent lonidamine', *Journal of Biological Chemistry*. doi: 10.1074/jbc.M115.697516.
23. Hägerhäll, C. (1997) 'Succinate: quinone oxidoreductases', *Biochimica et Biophysica Acta (BBA) - Bioenergetics*. doi: 10.1016/s0005-2728(97)00019-4.
24. Hargreaves, I. P. *et al.* (2007) 'Inhibition of mitochondrial complex IV leads to secondary loss complex II-III activity: Implications for the pathogenesis and treatment of mitochondrial encephalomyopathies', *Mitochondrion*. doi: 10.1016/j.mito.2007.02.001.
25. Healey, K. R. and Perlin, D. S. (2018) 'Fungal resistance to echinocandins and the MDR phenomenon in Candida glabrata', *Journal of Fungi*. doi: 10.3390/jof4030105.
26. Hu, Z. *et al.* (2016) 'Mitochondrial defects confer tolerance against cellulose deficiency', *Plant Cell*. doi: 10.1105/tpc.16.00540.
27. Hytti, M. *et al.* (2019) 'Antimycin A-Induced Mitochondrial Damage Causes Human RPE Cell Death despite Activation of Autophagy', *Oxidative Medicine and Cellular Longevity*. doi: 10.1155/2019/1583656.
28. Kitajima-Ihara, T. and Yagi, T. (1998) 'Rotenone-insensitive internal

NADH-quinone oxidoreductase of Saccharomyces cerevisiae mitochondria: The enzyme expressed in Escherichia coli acts as a member of the respiratory chain in the host cells', *FEBS Letters*. doi: 10.1016/S0014-5793(97)01533-0.
29. Koszul, R. *et al.* (2003) 'The complete mitochondrial genome sequence of the pathogenic yeast Candida (Torulopsis) glabrata', *FEBS Letters*. doi: 10.1016/S0014-5793(02)03749-3.
30. Kullberg, B. J. and Arendrup, M. C. (2015) 'Invasive candidiasis', *New England Journal of Medicine*. doi: 10.1056/NEJMra1315399.
31. Kregiel, D. (2012) 'Succinate Dehydrogenase of Saccharomyces cerevisiae – The Unique Enzyme of TCA Cycle – Current Knowledge and New Perspectives', in *Dehydrogenases*. doi: 10.5772/48413.
32. Kuranda, K. *et al.* (2006) 'Investigating the caffeine effects in the yeast Saccharomyces cerevisiae brings new insights into the connection between TOR, PKC and Ras/cAMP signalling pathways', *Molecular Microbiology*. doi: 10.1111/j.1365-2958.2006.05300.x.
33. Leadsham, J. E. and Gourlay, C. W. (2010) 'CAMP/PKA signaling balances respiratory activity with mitochondria dependent apoptosis via transcriptional regulation', *BMC Cell Biology*. doi: 10.1186/1471-2121-11-92.
34. Leavesley, H. B. *et al.* (2008) 'Interaction of cyanide and nitric oxide with cytochrome c oxidase: Implications for acute cyanide toxicity', *Toxicological Sciences*. doi: 10.1093/toxsci/kfm254.
35. Li, D. *et al.* (2011) 'Enzymatic dysfunction of mitochondrial complex i of the candida albicans goa1 mutant is associated with increased reactive oxidants and cell death', *Eukaryotic Cell*. doi: 10.1128/EC.00303-10.
36. Liao, X. S. *et al.* (1991) 'Intramitochondrial functions regulate nonmitochondrial citrate synthase (CIT2) expression in Saccharomyces cerevisiae.', *Molecular and Cellular Biology*. doi: 10.1128/mcb.11.1.38.
37. Montagna, M. T. *et al.* (2014) 'Candidemia in Intensive Care Unit: A nationwide prospective observational survey (GISIA-3 study) and review of the European literature from 2000 through 2013', *European Review for Medical and Pharmacological Sciences*.
38. Niimi, K. *et al.* (2006) 'Overexpression of Candida albicans CDR1, CDR2, or MDR1 does not produce significant changes in echinocandin susceptibility', *Antimicrobial Agents and Chemotherapy*. doi: 10.1128/AAC.50.4.1148-1155.2006.
39. Parsons, D. W. *et al.* (2008) 'An Integrated Genomic Analysis of', *Science*.
40. Pfaller, M. A. and Diekema, D. J. (2007) 'Epidemiology of invasive candidiasis: A persistent public health problem', *Clinical Microbiology Reviews*. doi: 10.1128/CMR.00029-06.
41. Philip, B. and Levin, D. E. (2001) 'Wsc1 and Mid2 Are Cell Surface Sensors for Cell Wall Integrity Signaling That Act through Rom2, a Guanine Nucleotide Exchange Factor for Rho1', *Molecular and Cellular Biology*. doi: 10.1128/mcb.21.1.271-280.2001.
42. Public Health England (2017) 'Voluntary surveillance of candidaemia in England , Wales and Northern Ireland', *Health protection Report [serial online]*.

43. Qin, Y. *et al.* (2019) 'Heterogeneity in respiratory electron transfer and adaptive iron utilization in a bacterial biofilm', *Nature Communications*. doi: 10.1038/s41467-019-11681-0.
44. Rai, M. N. *et al.* (2012) 'Functional Genomic Analysis of Candida glabrata-Macrophage Interaction: Role of Chromatin Remodeling in Virulence', *PLoS Pathogens*. doi: 10.1371/journal.ppat.1002863.
45. Ramage, G. *et al.* (2012) 'Fungal biofilm resistance', *International Journal of Microbiology*. doi: 10.1155/2012/528521.
46. Rodrigues, M. L. (2018) 'The multifunctional fungal ergosterol', *mBio*. doi: 10.1128/mBio.01755-18.
47. Rosen, R. *et al.* (2004) 'Probing the active site of homoserine trans-succinylase', *FEBS Letters*. doi: 10.1016/j.febslet.2004.10.037.
48. Ruy, F., Vercesi, A. E. and Kowaltowski, A. J. (2006) 'Inhibition of specific electron transport pathways leads to oxidative stress and decreased Candida albicans proliferation', *Journal of Bioenergetics and Biomembranes*. doi: 10.1007/s10863-006-9012-7.
49. Samokhvalov, V., Ignatov, V. and Kondrashova, M. (2004) 'Inhibition of Krebs cycle and activation of glyoxylate cycle in the course of chronological aging of Saccharomyces cerevisiae. Compensatory role of succinate oxidation', *Biochimie*. doi: 10.1016/j.biochi.2003.10.019.
50. Sharma, L., Lu, J. and Bai, Y. (2009) 'Mitochondrial Respiratory Complex I: Structure, Function and Implication in Human Diseases', *Current Medicinal Chemistry*. doi: 10.2174/092986709787846578.
51. She, X. *et al.* (2015) 'Fungal-specific subunits of the Candida albicans mitochondrial complex I drive diverse cell functions including cell wall synthesis', *Cellular Microbiology*. doi: 10.1111/cmi.12438.
52. Shingu-Vazquez, M. and Traven, A. (2011) 'Mitochondria and fungal pathogenesis: Drug tolerance, virulence, and potential for antifungal therapy', *Eukaryotic Cell*. doi: 10.1128/EC.05184-11.
53. Silva, S. *et al.* (2009) 'Biofilms of non-Candida albicans Candida species: Quantification, structure and matrix composition', *Medical Mycology*. doi: 10.3109/13693780802549594.
54. Silva, S. *et al.* (2012) 'Candida glabrata, Candida parapsilosis and Candida tropicalis: Biology, epidemiology, pathogenicity and antifungal resistance', *FEMS Microbiology Reviews*. doi: 10.1111/j.1574-6976.2011.00278.x.
55. Sun, F. *et al.* (2005) 'Crystal structure of mitochondrial respiratory membrane protein Complex II', *Cell*. doi: 10.1016/j.cell.2005.05.025.
56. Sun, N. *et al.* (2019) 'Unique, diverged, and conserved mitochondrial functions influencing candida albicans respiration', *mBio*. doi: 10.1128/mBio.00300-19.
57. Sundstrom, P. (2002) 'Adhesion in Candida spp', *Cellular Microbiology*. doi: 10.1046/j.1462-5822.2002.00206.x.
58. Torres, J. *et al.* (2002) 'Regulation of the cell integrity pathway by rapamycin-sensitive TOR function in budding yeast', *Journal of Biological Chemistry*. doi: 10.1074/jbc.M205408200.
59. Vermitsky, J. P. and Edlind, T. D. (2004) 'Azole resistance in Candida glabrata: Coordinate upregulation of multidrug transporters and evidence

for a Pdr1-like transcription factor', *Antimicrobial Agents and Chemotherapy*. doi: 10.1128/AAC.48.10.3773-3781.2004.
60. Vermitsky, J. P. *et al.* (2006) 'Pdr1 regulates multidrug resistance in Candida glabrata: Gene disruption and genome-wide expression studies', *Molecular Microbiology*. doi: 10.1111/j.1365-2958.2006.05235.x.
61. Watanabe, T. *et al.* (2006) 'Hyphal formation of Candida albicans is controlled by electron transfer system', *Biochemical and Biophysical Research Communications*. doi: 10.1016/j.bbrc.2006.07.066.
62. Weinert, B. T. *et al.* (2013) 'Lysine succinylation is a frequently occurring modification in prokaryotes and eukaryotes and extensively overlaps with acetylation', *Cell Reports*. doi: 10.1016/j.celrep.2013.07.024.
63. Wojtovich, A. P. *et al.* (2013) 'Physiological consequences of complex II inhibition for aging, disease, and the mKATP channel', *Biochimica et Biophysica Acta - Bioenergetics*. doi: 10.1016/j.bbabio.2012.12.007.
64. Xia, M. F. *et al.* (2019) 'Communication between mitochondria and other organelles: a brand-new perspective on mitochondria in cancer', *Cell and Bioscience*. doi: 10.1186/s13578-019-0289-8.
65. Xie, Z. *et al.* (2012) 'Lysine succinylation and lysine malonylation in histones', in *Molecular and Cellular Proteomics*. doi: 10.1074/mcp.M111.015875.
66. Yamashita, K. *et al.* (2019) 'The Novel Arylamidine T-2307 Selectively Disrupts Yeast Mitochondrial Function by Inhibiting Respiratory Chain Complexes', *Antimicrobial Agents and Chemotherapy*. doi: 10.1128/aac.00374-19.

Appendix

Appendix 1 – *C. glabrata* clinical Isolate growth curve data

A

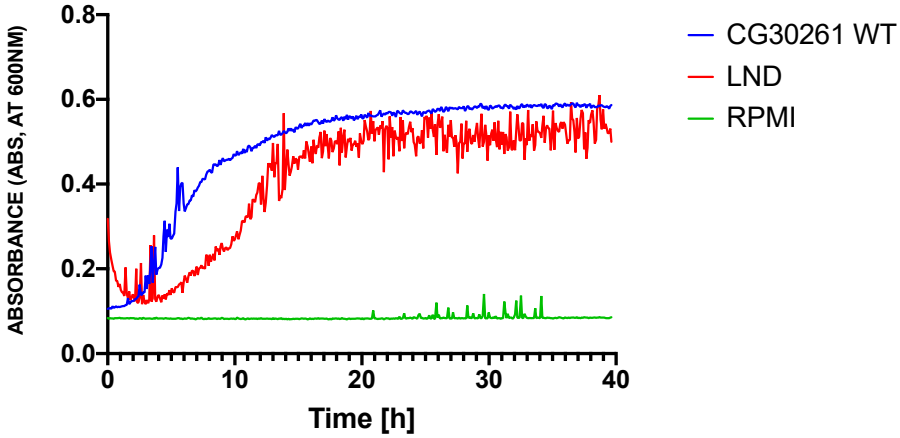

B

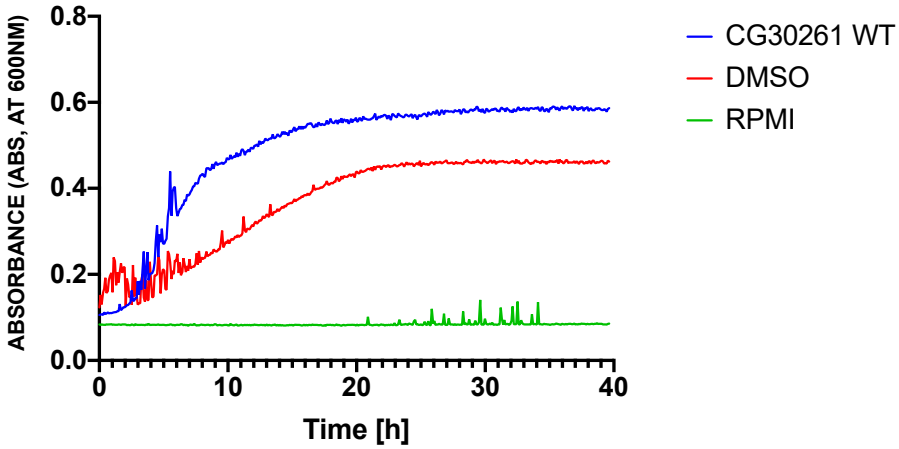

C

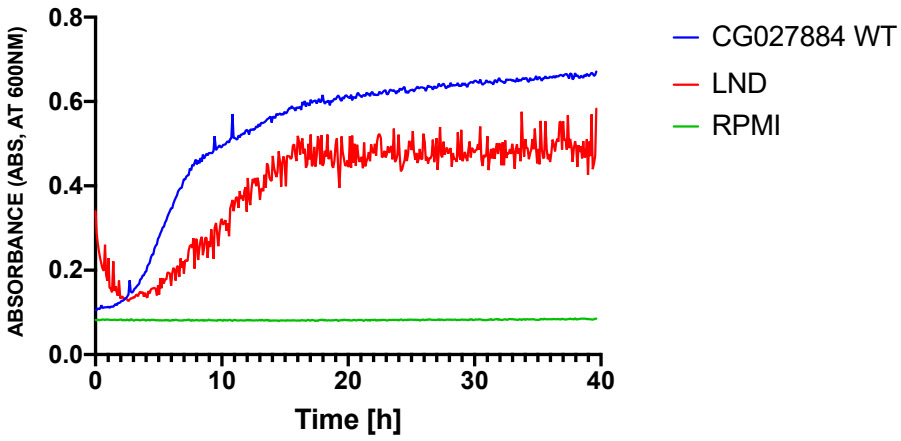
ABSORBANCE (ABS, AT 600NM)
0.0
0.2
0.4
0.6
0.8
0
10
20
30
40
Time [h]
CG027884 WT
LND
RPMI

D

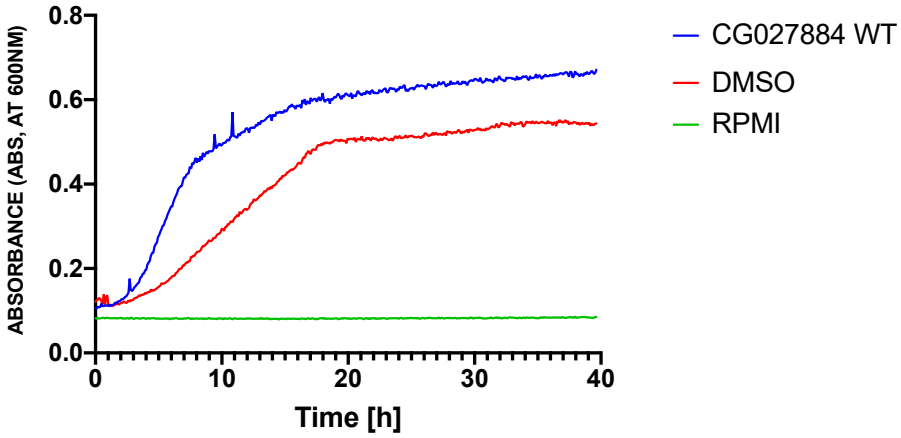
ABSORBANCE (ABS, AT 600NM)
0.0
0.2
0.4
0.6
0.8
0
10
20
30
40
Time [h]
CG027884 WT
DMSO
RPMI

E

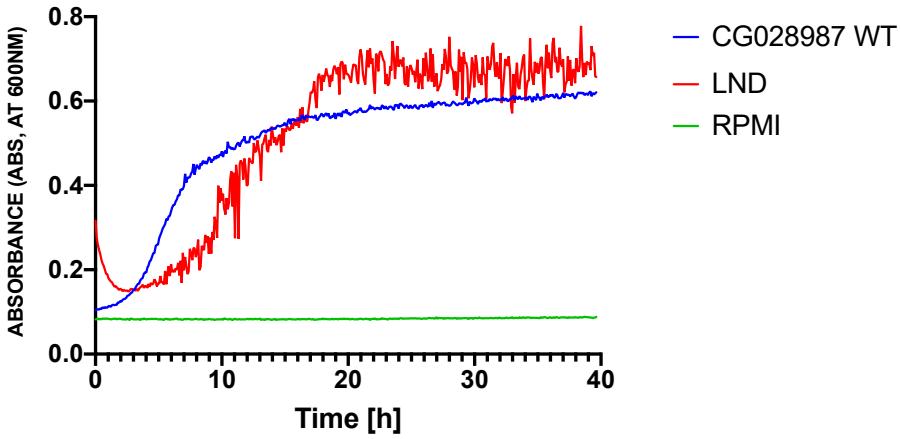
ABSORBANCE (ABS, AT 600NM)
0.0
0.2
0.4
0.6
0.8
0
10
20
30
40
Time [h]
CG028987 WT
LND
RPMI

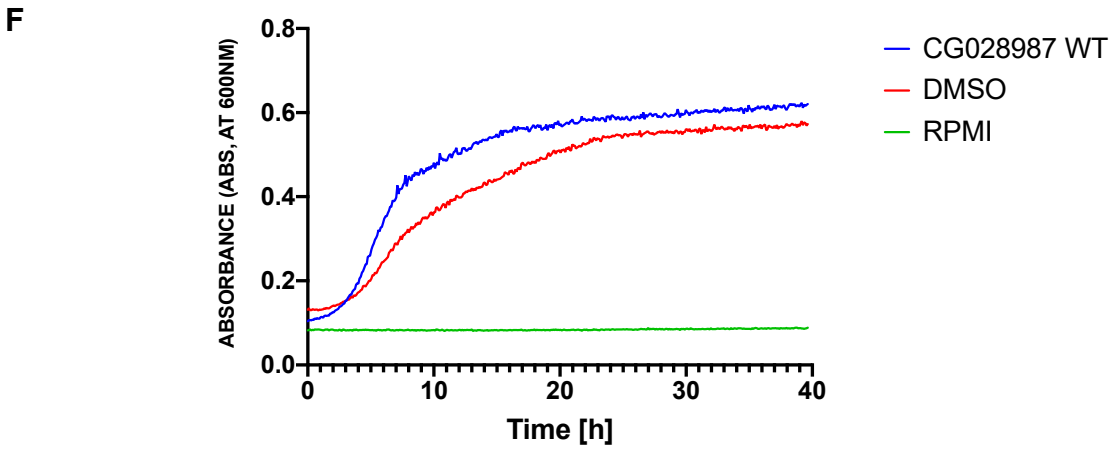

Fig 29. Growth assays of *C. glabrata* clinical isolates with LND and DMSO in RPMI media over 40 hours. (A) Clinical isolate 30261 WT growth comparison with LND treated cells. (B) Clinical isolate 30261 WT growth comparison with DMSO treated cells. (C) Clinical isolate 027884 WT growth comparison with LND treated cells. (D) Clinical isolate 027884 WT growth comparison with DMSO treated cells. (E) Clinical isolate 028987 WT growth comparison with LND treated cells. (F) Clinical isolate 028987 WT growth comparison with DMSO treated cells.

Appendix 2 – *S. Cerevisiae* WT and TCA mutant growth assays with TTFA

A

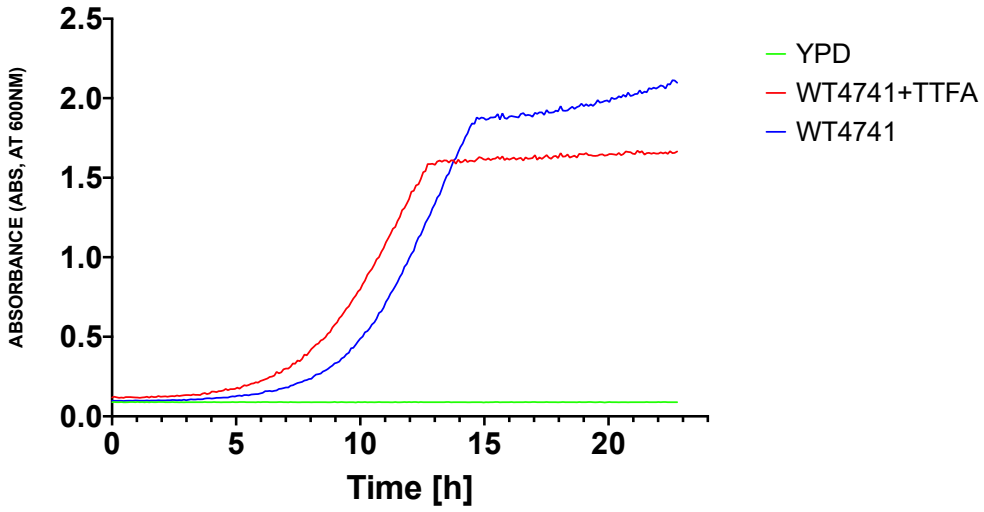

B

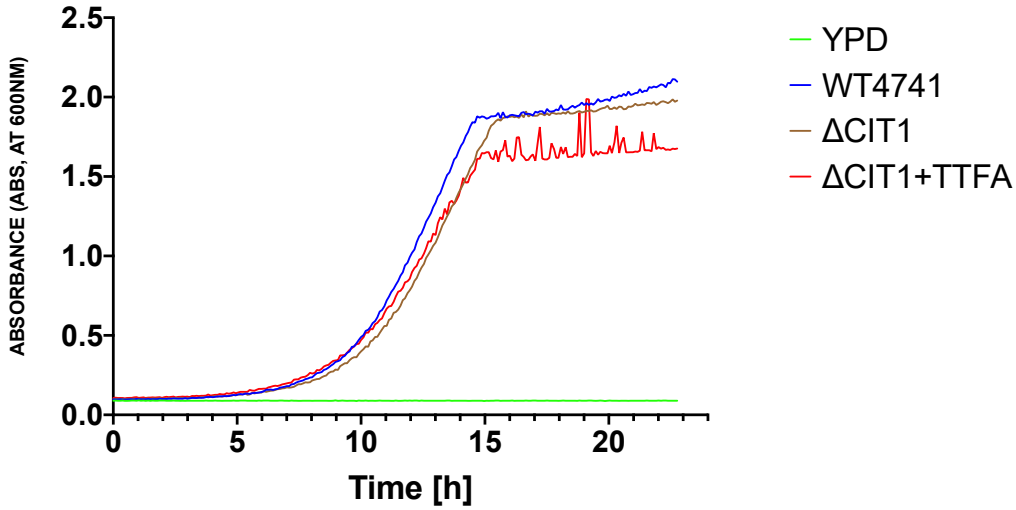

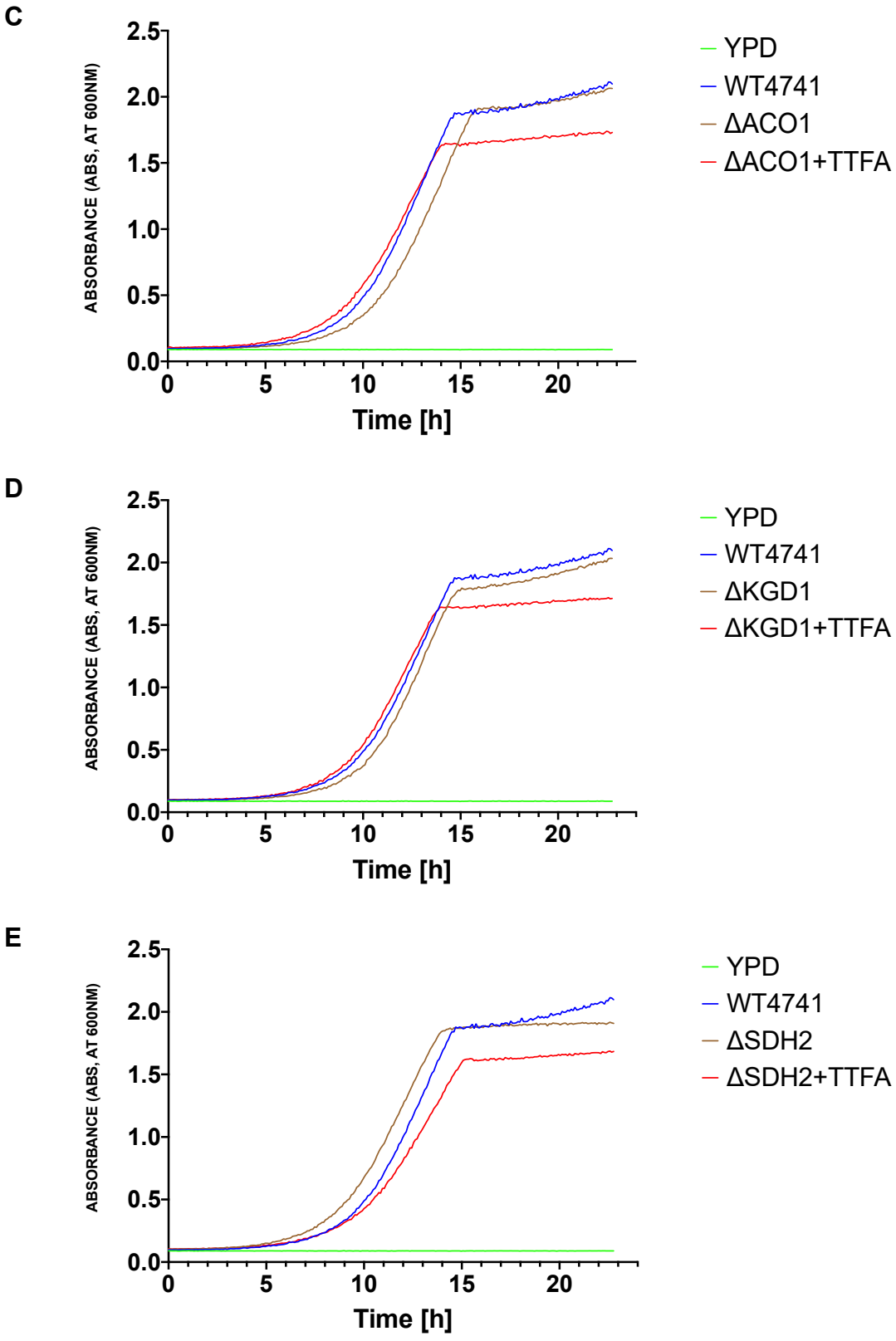

Fig 30. Growth assays of *S. Cerevisiae WT4741* and TCA mutants with TTFA in YPD media over 24 hours. (A)*WT* (B)Δ*cit1* (C)Δ*aco1* (D)Δ*kgd1* (E)Δ*sdh2*